CHALMERS

Coordinated Control of Wind and Hydro to Provide Grid Fast Frequency Support

Master's thesis in Electric Power Engineering

Ahmed Sunjaq

Department of Electrical Engineering
Division of Electric Power Engineering
CHALMERS UNIVERSITY OF TECHNOLOGY
Gothenburg, Sweden 2020

MASTER'S THESIS 2020

Coordinated Control of Wind and Hydro to Provide Grid Fast Frequency Support

Ahmed Sunjaq

CHALMERS
UNIVERSITY OF TECHNOLOGY

Department of Electrical Engineering
Division of Electric Power Engineering
CHALMERS UNIVERSITY OF TECHNOLOGY
Gothenburg, Sweden 2020

Coordinated Control of Wind and Hydro to Provide Grid Fast Frequency Support
Ahmed Sunjaq

Supervisor/examiner: Peiyuan Chen, Electric Power Engineering

Master's Thesis 2020
Department of Electrical Engineering
Division of Electric Power Engineering
Chalmers University of Technology
SE-412 96 Gothenburg
Telephone +46 31 772 1000

Typeset in LaTeX
Gothenburg, Sweden 2020

Coordinated Control of Wind and Hydro to Provide Grid Fast Frequency Support
Ahmed Sunjaq
Department of Electrical Engineering
Chalmers University of Technology

Abstract

The inertia of the Nordic power system (NPS) is reducing due to the replacement of large nuclear units and fossil fuel powered thermal units with converter-interfaced wind turbines (WTs). This project aims to investigate the possibility of providing a joint service of coordinated fast frequency support from hydro units and WTs in a low inertia power system. While WTs can arrest the initial frequency fall by providing fast support using their converter controllers, hydro turbines are capable of mitigating the second frequency dip (SFD) resulting from the restoration phase of WTs by increasing their production accordingly. Results show that the SFD severity depends on the fast frequency reserve (FFR) characteristics. In case of a rate-of-change-of-frequency-based FFR support, the SFD can be solved by delaying the recovery and limiting its power. On the other hand, a grid-code-based FFR may cause a severe SFD and, thus, requires coordination. This may imply that the current grid code is not suitable to avoid the SFD problem especially that WTs will take a larger part of the frequency regulation in the future.

Keywords: WTs, Hydro turbines, Fast frequency reserve, Primary frequency control, Coordination, Initial frequency dip, Secondary frequency dip.

Acknowledgements

I would like to express my very great gratitude to my supervisor/examiner Assoc. Prof. Peiyuan Chen for his guidance and constructive feedback, for providing valuable literature and for always being available when needed.

A big thanks to Senior Scientist Evert Agneholm from Protrol AB for answering questions regarding frequency regulation practices in the Nordic power system.

A special thanks to Chalmers University for offering me an IPOET scholarship funded by the Swedish Council for Higher Education, without them I would not be here.

I would like to also thank my family and friends for supporting me all the time.

Ahmed Sunjaq, Gothenburg, June 2020

Contents

List of Figures

List of Tables

1

Introduction

1.1 Background

Frequency stability is one of the biggest concerns in power systems. A significant deviation of frequency from its nominal value may cause mechanical problems to rotating machines and a fast frequency drop may trip HVDC lines and wind farms equipped with rate-of-change-of-frequency (RoCoF) based relays. For this reason, transmission system operator (TSO) has the responsibility of maintaining frequency as close as possible to the nominal value by balancing generation and demand in a continuous manner. To fulfill the target set to reduce CO2 emission, the electricity sector has been undergoing a transformation towards renewable generators such as wind turbines (WTs) and photovoltaic (PV) cells, which are power-electronic converter interfaced rather than synchronous-based generation. Furthermore, there is an increased percentage of converter-interfaced loads compared to directly connected induction machines, and much more HVDC lines are being installed. These changes are expected to result in a system with less kinetic energy in the form of rotating masses, less frequency reserve than before, and requires more balancing due to the intermittency of renewable energy resources. All these reasons combined will lead to a system that is less immune to disturbances. This issue can be mitigated by providing a reserve with larger volume or a reserve that can be activated in a faster manner. Hydro units are the main resource of frequency containment reserve (FCR) in the Nordic synchronous area (NSA), but they have a relatively slow ramp rate, especially the ones in Sweden with low head, which makes their FCR provision less effective in grid frequency support, particularly, in a system with low inertia constant, where the rate of change of frequency (RoCoF) is relatively high. On the other hand, variable speed wind turbines (VSWTs) are capable of boosting up their output power very fast via their converter interface, but their fast frequency reserve (FFR) provision cannot be sustained for a long period and they have to restore their rotating speed to avoid stall and to go back to maximum power point tracking (MPPT). This restoration process, if not executed properly may pull down the frequency even more. This project intends to tackle this issue on second frequency dip (SFD) that can be potentially caused by the recovery of VSWTs after providing FFR.

1.2 Aim

The main objective of the project is to develop and evaluate a coordinated control strategy between hydro and wind units for FFR and FCR provision that has the ability to reduce the initial frequency fall and mitigate the SFD due to the restoration of WTs.

1.3 Tasks and methodology

First of all, a review is carried out to study technical requirements of FFR and FCR provisions in the NSA. This shall give a detailed understanding of limitations set by the regulations. For this task, reports [1, 2, 3], which are issued by the TSOs of the NSA, are reviewed.

Second problem in hand is to model VSWTs and hydro turbines in simulink including both, plant and control models. Transfer function based model is used for the mathematical representation of both models, which is suitable for simulation purposes. Kaplan model is utilized for the representation of hydro models in the NSA since it constitutes the majority of newly built turbines in Sweden. The model is simplified to a linear model that has a speed-droop governor control, an actuator and a penstock and turbine model. While for the VSWT, the model in [5] is used for this project, which is a 3.6 MW WT made by General Electric (GE). This model is more complicated compared to the hydro turbine because there are many controls inside the VSWT model such as the speed control, pitch control and pitch compensation. Furthermore, an inertia provision block is added for WTs to provide FFR during a disturbed operation. Hydro and wind models in this task are aggregated units that represent the capacity in the NSA and thus they should be scaled up to reflect this fact.

The third task is the core of the project, to develop a coordinated control strategy between hydro and wind units for FFR and FCR provision. Performance of the developed method will be evaluated under a dimensioning fault and a 2040 windy summer scenario is considered, where the system has a very low inertia. First, the generation in 2040 is estimated based on the installed capacities in the NSA in 2019 and in 2040 based on different scenarios. The system is modeled using the swing equation, where the inertia of the system and its damping constant plays the main role in the frequency response. To facilitate the problem in hand, it is broken up into three case studies:

- Considering only hydro units contributing to primary frequency control.
- Both WTs and hydro units providing frequency support.
- Establishing a communication channel between hydro and wind turbines to provide coordinated control.

Hydro units can have different governor settings based on the producer. Therefore, a study is made on different governor settings and their impact on the system frequency response. The FFR properties should be identified, which involve the activation frequency, shape of response and its duration and the restoration time. In this project, a RoCoF-based inertia provision and a predetermined support shape are utilized, both being evaluated separately. Then the system SFD is evaluated with respect to different FFR capacities and settings to identify the cases where coordination is really needed. Coordination is then established such that hydro units boost up their production in correspondence with the restoration phase of WTs.

1.4 Scope

To facilitate the problem analysis within the thesis time frame, some assumptions are made:

- The WT's rotor model is simplified into a one mass model in which the turbine and the generator are considered as one rigid body. Moreover, the electrical part of the wind model is neglected since the electrical transients are much faster than the mechanical dynamics. Furthermore, voltage at the terminals of the turbine is assumed 1 pu when calculating the electrical current reference for the power converter.
- Non-linear elements of the hydro model are neglected to make the analysis easier. Moreover, hydro capacity in the NSA is aggregated into a Kaplan unit although there are other types used in the NSA like Francis and Pelton. However, Kaplan is the most common type of turbines built nowadays in Sweden and that is why we focus on it in this project.
- The power system is represented using the simplified swing equation model, where small perturbations in power are assumed. The load frequency dependence constant is assumed similar to the current parameters of the system. Although, it is expected that the future power system will have more converter connected loads, which imply that less load frequency dependence will be available.

1.5 Sustainable aspects

In this section, the sustainable aspects corresponding to this project are discussed. These aspects reflect upon the economical, ecological and social effects. With the increased share of weather-based renewable generation, more reserve capacity in the system are needed to keep power balance in the system. But the usage of the energy stored in the blades of a WT can provide fast frequency reserve to the system without additional equipment investment. Moreover, by using WTs as a source of reserve, this will allow us to reduce the dependency on steam turbines that use fossil fuel as a source of energy. This would reduce the CO2 emissions in air, and thus, mitigate the greenhouse effect. As a consequence, the society will have cleaner air, less global warming than before and probably decrease the phenomena of burning forests. In a technical point of view, the project is expected to improve the frequency stability in the power system, and hence, less outages are expected to occur. As a result, the quality of life would increase. In the overall, the project is expected to have a positive impact on sustainable aspects in all of its three pillars.

1.6 Ethical dilemmas

Ethical aspects must be taken seriously when dealing with any project especially if it contains technical design. If VSWT plants are owned by different parties, there may be a conflict pursuing both sides to cooperate together to provide frequency support. Moreover, the potential consequences of the developed controller should be explained. This may include an excessive torque applied on the rotating blades during frequency support.

2

On Inertia and Frequency Regulation

2.1 Inertia

Inertia is the ability of a power system to resist changes in frequency due to the kinetic energy stored in the rotating mass of generators [7]. The inertia can be pictured as the kinetic energy stored in the system. The inertia constant of a single machine is given by

$$H = \frac{\frac{1}{2}J\Omega^2}{S_\mathrm{r}} \tag{2.1}$$

where J is the moment of inertia of the generator in Kg.m^2, Ω is the mechanical speed of the rotor in rad/s, S_r is the rated power of the generator in VA and H is the inertia constant in s. The inertia constant is the amount of time that is needed for the generator to transfer its kinetic energy into electrical energy when a load equal to its rated power is connected at its terminals. Assuming all generators in a power system are lumped in one single model, the equivalent inertia constant of the system is calculated as

$$H_\mathrm{sys} = \frac{\sum_{n=1}^{N} H_n S_{\mathrm{r},n}}{\sum_{n=1}^{N} S_{\mathrm{r},n}} \tag{2.2}$$

where N is the number of generators in the system and H_sys is the equivalent inertia constant of the system in s. Table 2.1 shows the typical values of inertia constant of different power plants. Although, VSWTs do not provide inertial response in their default control setting, but they have the ability to supply a temporary active power support similar to the inertial response of synchronous generators, as will be seen in Section 2.3.

Table 2.1: The typical inertia constant of different power plants [8]

Type of generation	H
Nuclear power plants	5-8 s
Other thermal units	2-7 s
Hydro units	2-4 s
Wind turbines	2.4-6 s

2.2 Frequency regulation

The dynamic behavior of the frequency of a power system is determined by the mechanical speed of synchronously-connected generators, which are governed by the swing equation

$$\frac{d\omega_\mathrm{r}}{dt} = \frac{(P_\mathrm{m} - P_\mathrm{e})}{2H_\mathrm{sys}\,\omega_\mathrm{r}} \tag{2.3}$$

where P_m is the mechanical power provided by generators given in pu, P_e is the electrical load in pu and ω_r is the frequency of the system in pu. When a mismatch in power occurs, for instance, a power plant is tripped, the frequency will drop down quickly. Initially, the extra power is provided from generators that are closest in terms of electrical distance (impedance). Then, the power is shared between production plants in proportion to their inertia. Until now, the extra power is being provided by the kinetic energy stored in the rotating masses, connected synchronously to the system, which is called inertial response. In the meanwhile, primary frequency control starts to take place, which has the responsibility of balancing the generation-load mismatch in order to restrain the drop of frequency. The primary frequency support is activated linearly with frequency deviation and the reserve is divided between the providers in proportion to their droop characteristics. Two services are offered by primary frequency support, the frequency containment reserve for normal operation (FCR-N), which is activated when the frequency is in the range [49.9, 50.1] Hz [3], and the frequency containment reserve for disturbed operation (FCR-D) which is upward regulated in the range [49.5, 49.9] Hz and downward regulated in the range [50.1, 50.5] Hz [2]. The primary frequency control is provided automatically by contracted spinning reserve in the system. After frequency has stabilized, there is a need to restore it back to 50 Hz. This is done first using secondary frequency control, or the so-called automatic frequency restoration reserve (aFRR) in the NSA. By changing the load reference set point automatically of generators that is intended to provide secondary support, it is possible to bring the frequency back to its nominal. Other purposes of secondary frequency control, is to release primary frequency control and maintain the scheduled power interchange between control areas. The secondary frequency control can be provided by non-spinning reserve also. Finally, the tertiary frequency control, or as called in the NSA, the manual frequency Restoration reserve (mFRR), replaces the secondary control. The purpose of this control, is to distribute the reserve between providers such that the operating costs are minimum. Figure 2.1 shows the different stages of frequency regulation as a function of time following a loss of a power plant.

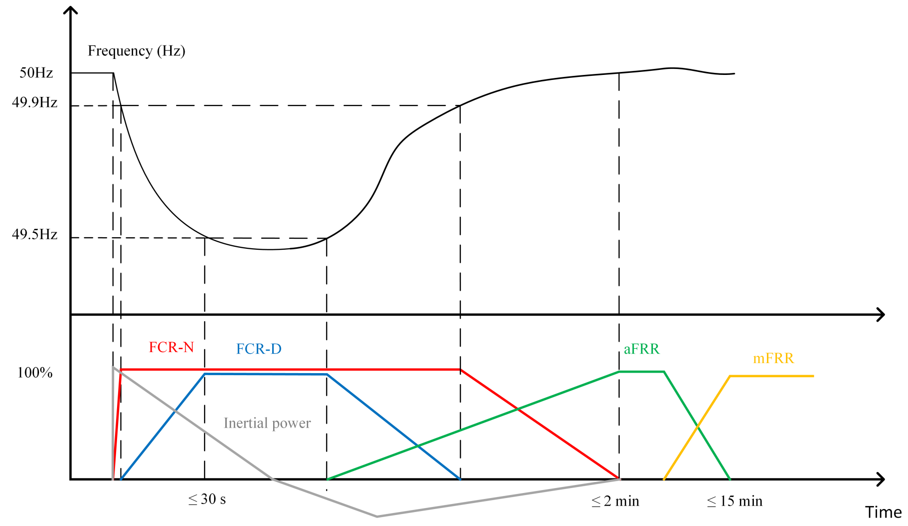

Figure 2.1: Frequency regulation types as a function of time following a sharp frequency decrease due to a loss of a power plant.

2.3 Fast Frequency Reserve (FFR)

From (2.3), it is concluded that a power system with lower inertia constant will definitely have a higher RoCoF for the same disturbance. To prevent the frequency from declining rapidly, a system with higher amount of reserve or a reserve that is activated faster is needed. The fast frequency reserve is used to mitigate the effect of low inertia systems on rapid frequency deviations as it has a very fast ramp rate but usually it comes with limited amount of energy depending on the technology used for providing it. It can be activated based on different logics and it can have a variety of shape response. For example, the power support can be proportional to frequency deviation as in FCR, proportional to the RoCoF as a conventional generator, then it is called synthetic inertia, or it might be independent on frequency like a predetermined step [7]. The choice of the characteristics of FFR provision depends mostly on the technology used for providing it. Table 2.2 lists the most popular options for FFR provision along with their properties.

Table 2.2: Different technologies for FFR provision and their properties [7].

Control: A: k df/dt (Synthetic inertia), B: KΔf, C: Predetermined power profile.

Technology property	Relay-connected load	converter-connected load	Wind power	Battery	HVDC
Activation time	instant	<0.5 s	<0.5 s	<0.5 s	<0.5 s
Duration	Minutes	Minutes	10% for about 10 s	Minutes	N/A
Control	C	B, C	A, B, C	A, B, C	A, B, C

2.4 FCR technical requirements

To be able to deliver FCR service, the concerned entity should be prequalidied first from the TSO they are connected to [2, 3]. In this section, the technical requirements of FCR-N and FCR-D reserves are demonstrated.

2.4.1 FCR-N requirements

The FCR-N is activated during normal operation, when the frequency is between 49.9 Hz and 50.1 Hz [3]. When the frequency is below 50 Hz, generators increase their production while controllable loads reduce their consumption, and vice versa, when the frequency is over 50 Hz, generators reduce their production while loads increase their consumption. For frequencies equal to 49.9 Hz and below, the FCR-N upward capacity is activated completely, and for frequencies equal to 50.1 Hz and above, the downward regulation capacity of FCR-N is activated. The FCR-N steady state response should be linear with respect to the frequency deviation, see Figure 2.2. In case of a rapid frequency change to 49.9 HZ or 50.1 Hz, then the FCR-N should be fully activated within 2-3 minutes [9].

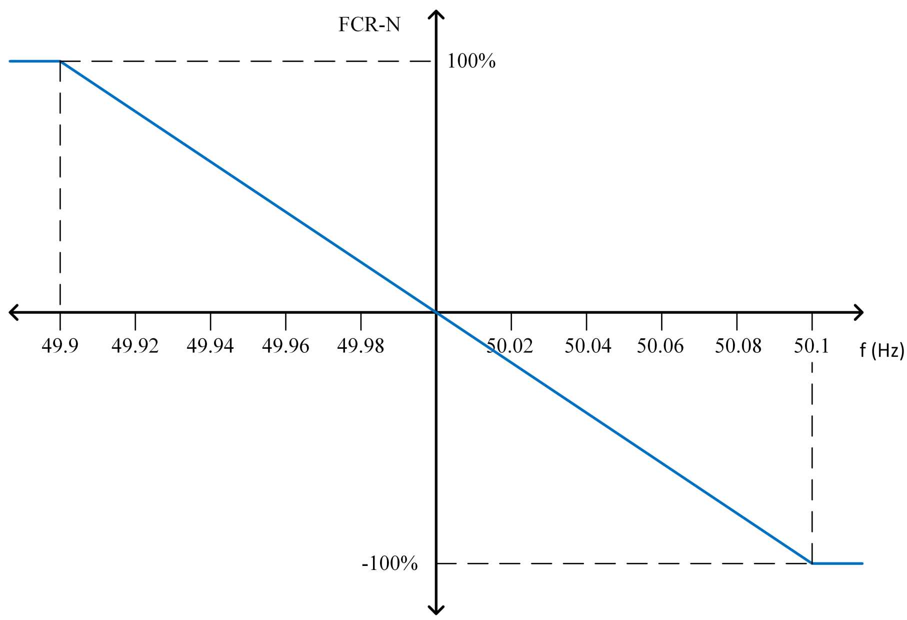

Figure 2.2: FCR-N provision steady state characteristics.

The FCR-N reserve in the NSA should not be less than 600 MW [9]. These are distributed between the subsystems of the NSA in proportion to the annual consumption of each area. Table 2.3 shows the reserve distribution between NSA subsystems.

Table 2.3: The FCR-N Distribution between subsystems of the NSA (2013) [9].

	Annual consumption 2013 (TWh)	**FCR-N Reserve (MW)**
Eastern Denmark	13.7	22
Finland	85.2	138
Norway	130.0	210
Sweden	142.5	230
NSA	**371.4**	**600**

2.4.2 FCR-D requirements

The FCR-D is activated when the frequency goes out of the range [49.9, 50.1] Hz [2]. When the frequency is equal to or below 49.5 Hz, the upward regulation capacity of the FCR-D is fully activated. When the frequency is equal to or above 50.5 Hz, the downward regulation capacity is fully activated. The FCR-D should be linearly proportional to the frequency deviation in the periods [49.5, 49.9] Hz and [50.1 , 50.5] Hz, see Figure 2.3. In case of a rapid frequency drop to 49.5 Hz, 50% of the FCR-D capacity should be activated in less than 5 seconds, and 100% is activated in less than 30 seconds [9].

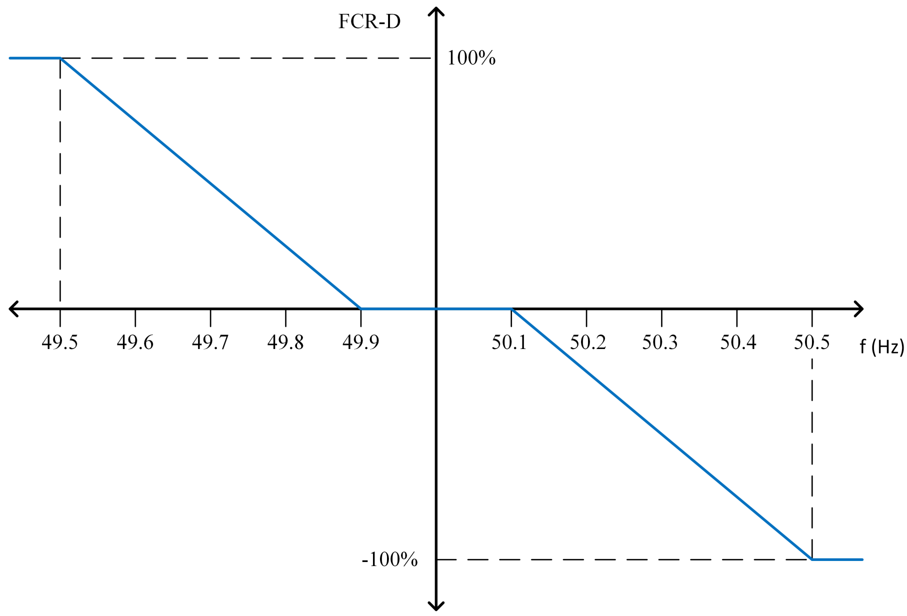

Figure 2.3: FCR-D provision steady state characteristics.

The FCR-D in the NSA should be greater than or equal to the dimensioning fault in the system, minus the load frequency dependence [9]. The dimensioning fault should comply to the N-1 criteria, which means that the largest disturbance possible to occur in a system is considered as the dimensioning fault of that system. In the NSA, the dimensioning fault is the trip of 1400 MW Oskarshamn 3 nuclear station. The load frequency dependence in the NSA is 400 MW/Hz, thus, the load is reduced by 200 MW when the frequency drops to 49.5 Hz. Therefore, a minimum of 1200 MW FCR-D is needed in the NSA. The

FCR-D distribution between subsystems of the NSA is proportional to the dimensioning fault in each area, see Table 2.4.

Table 2.4: The FCR-D distribution in the NSA (2013) [9].

	Dimensioning faults (MW)	FCR-D (MW)
Denmark	600	176.5
Finland	880	258.8
Norway	1200	352.9
Sweden	1400	411.8
Total	**1400**	**1200**

2.5 FFR technical requirements

In order to be able to deliver FFR service, the provider should be prequalified from the TSO, which is determined by a test to ensure that the entity is following the technical requirements [1]. Each cycle of FFR provision contains five main stages, Activation, support, deactivation, buffer and the recovery, then it repeats. Figure 2.4 shows one whole cycle of FFR provision.

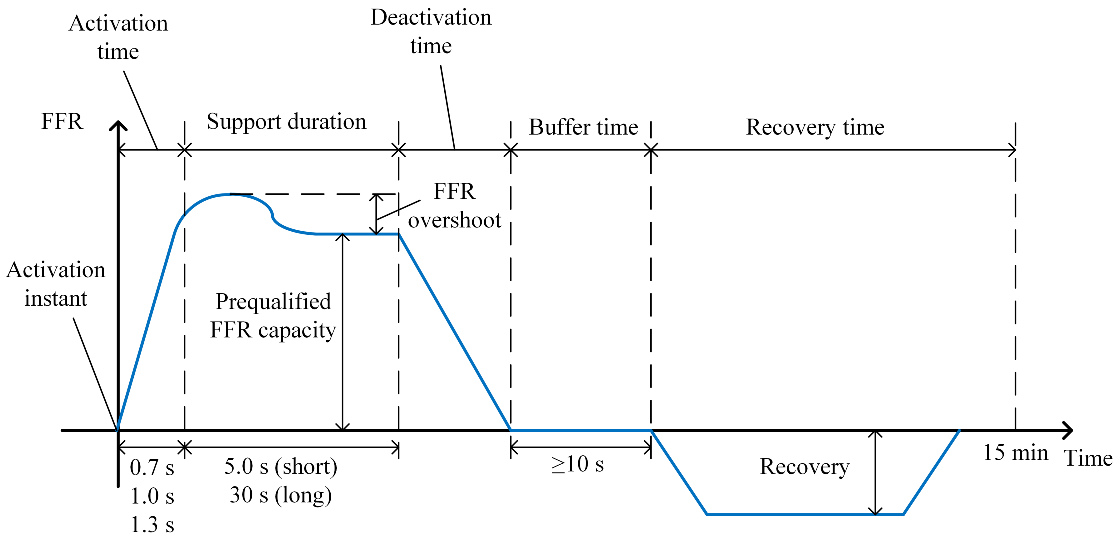

Figure 2.4: One cycle of FFR provision.

2.5.1 Activation and support periods

The following bullet points summarize the FFR activation and support requirements [1].

- The FFR is activated based on the frequency deviation and there are three alternative options with each having different requirements for the maximum full activation time, shown in Table 2.5. The period through which the FFR is ramped up towards the prequalified FFR capacity is called the activation period.

- The activation shape has no requirements, that means it can be anything as long as it fulfils the maximum activation time requirements, e.g., step, ramp, etc.
- Maximum allowable overshoot is 35%.
- The provider should be able to keep their prequalified FFR capacity for at least 5 s if they are committed to short support duration, or at least 30 s if they are committed to long support duration. This period is called the support period.
- There are no requirements on the shape of the support as long as the entity is capable of providing the prequalified FFR capacity for at least 5 or 30 s depending on their contract.
- The FFR provision may still be active if the frequency is below 49.8 Hz, but if the support duration of 5 s or 30 s has passed, the deactivation can start. However, when the frequency exceeds 49.8 Hz, the unit must deactivate within 15 minutes to be prepared for a new event.

Table 2.5: Three alternative plans of frequency activation levels [1].

Alternatives	Activation level (Hz)	Maximum full activation time (s)
A	49.7	1.3
B	49.6	1
C	49.5	0.7

2.5.2 Deactivation period

After the support duration ends, comes the deactivation period, through which, the providing entity reduces its reserve provision until it reaches zero. The technical requirements of this period are listed below [1].

- The FFR during deactivation should not exceed the maximum FFR from the activation instant till the end of the support duration.
- The deactivation shape has different requirements for short and long support providing entities.
  - Long support duration: there are no requirements on the deactivation shape, e.g, it can be step-wise.
  - Short support duration: the average rate of deactivation should be less than 20% of the prequalified FFR capacity per second over any time period of one second.

2.5.3 Recovery period

Some units need to recover after each FFR providing cycle, like WTs for instance. The recovery period has also its rules that need to be followed, these are presented below [1].

- The recovery period should not start before the deactivation has ended plus 10 s.
- There are no requirements on the recovery shape, e.g., it may be sharp.
- The recovery magnitude can not exceed 25% of prequalified FFR capacity.
- The recovery period is not necessary after each cycle, it depends on the providing entity.

2.5.4 Repeatability

Each FFR providing entity must be ready for a new cycle of FFR provision after 15 minutes has passed from the activation instant [1]. But this rule does not apply if the frequency is below 49.8 Hz and the FFR is still active from the previous cycle.

3

Modeling of Synchronous-Machine Based Power System

3.1 Grid model

The power system for frequency studies is modeled using (2.3). By assuming small deviations in power, this equation can be approximated as

$$2H\frac{d\Delta\omega_r}{dt} \approx \Delta P_m - \Delta P_e \tag{3.1}$$

where ΔP_e is a small deviation in load in pu, ΔP_m is a small deviation in generation in pu and $\Delta\omega_r$ is a small deviation in grid frequency in pu. This equation specifies the frequency dynamics with respect to power deviations in the system instead of tuques, which is preferred in power system studies. The load is composed of two parts, frequency independent load and frequency dependent load. Thus, (3.1) can be expressed as

$$2H\frac{d\Delta\omega_r}{dt} \approx \Delta P_m - \Delta P_L - D\Delta\omega_r \tag{3.2}$$

where D is the load-damping constant in pu power per pu frequency. This equation is transformed into the Laplace domain and rearranged in the form of a transfer function as follows

$$\frac{\Delta\omega_r}{\Delta P_m - \Delta P_L} = \frac{1}{2Hs+D} \tag{3.3}$$

A block diagram representation of (3.3) is presented in Figure 3.1.

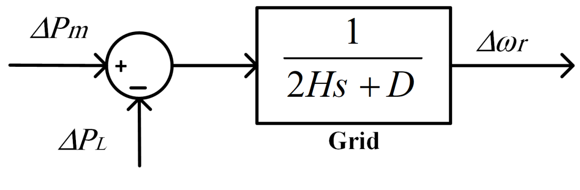

Figure 3.1: A block diagram representation of the approximate grid model.

3.2 Governor model

The governor is an essential component in any power plant that is responsible for frequency regulation. Most of the governors used in the power system are of speed-droop characteristics. The block diagram of such a governor is illustrated in Figure 3.2. The PI-controller would drive the steady state error signal to zero, this means

$$\omega_r^* - \omega_r - R\Delta P_m^* = 0$$

By rearranging this equation we get

$$R = \frac{\omega_r^* - \omega_r}{\Delta P_m^*} \tag{3.4}$$

where ω_r^* is the reference frequency in pu, ω_r is the measured frequency in pu, ΔP_m^* is the reference generator power in pu and R is the droop constant in pu frequency per pu power. According to (3.4), any change in frequency will not be compensated for completely and there will be a steady state frequency deviation. In steady state, (3.2) approaches zero, thus, by solving it simultaneously with (3.4), a formula of the steady state frequency deviation is found

$$\Delta\omega_{r,ss} = \frac{-\Delta P_L}{\frac{1}{R} + D} \tag{3.5}$$

Figure 3.3 shows the steady state speed-droop characteristics of such a governor system.

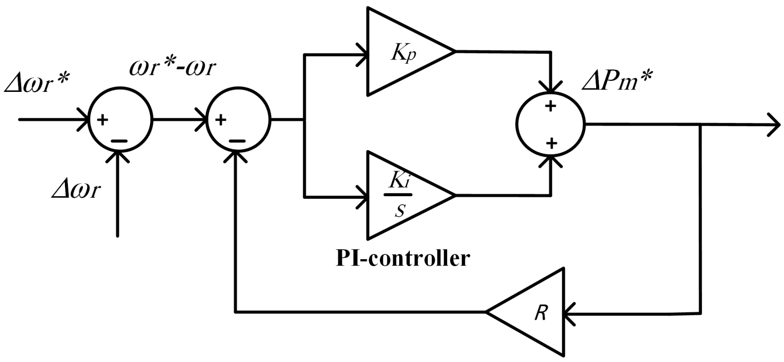

Figure 3.2: Block diagram of a speed-droop governor.

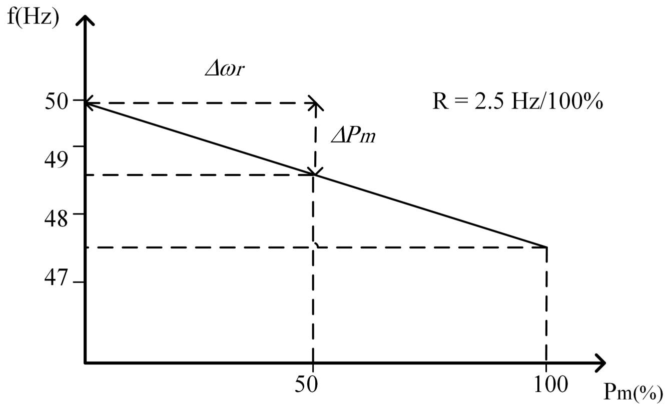

Figure 3.3: Steady state speed-droop characteristics.

In order to provide further controllability on the speed-droop characteristics, a load setpoint is added to the governor model as shown in Figure 3.4. In steady state the error signal approaches zero, hence, the following applies

$$\omega_r^* - \omega_r - R\Delta P_{droop}^* = 0$$

where

$$\Delta P_{droop}^* = \Delta P_m^* - \Delta P_L^*$$

This would allow the speed-droop characteristics to move upwards or downwards according to the reference setpoint value, as shown in Figure 3.5.

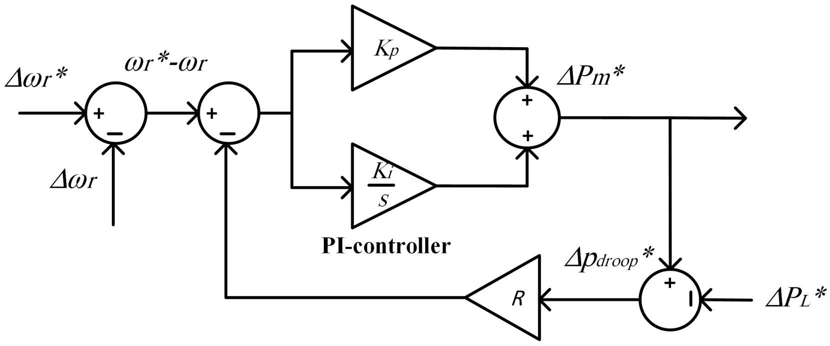

Figure 3.4: Speed-droop governor block diagram with load reference setpoint.

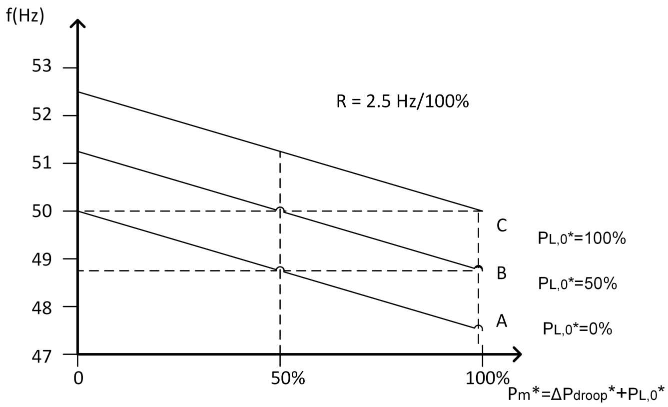

Figure 3.5: Steady state speed-droop characteristics with multiple setpoints.

The overall model of the system including the governor, plant and the grid is shown in Figure 3.6.

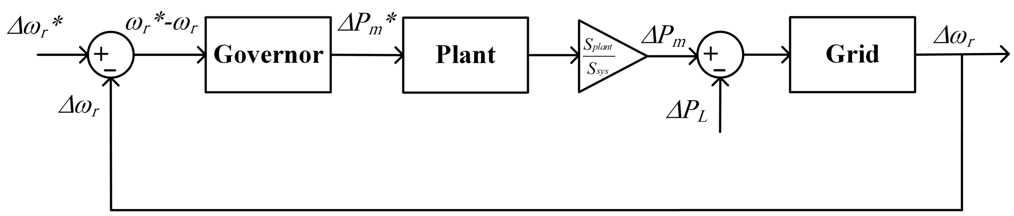

Figure 3.6: A block diagram of a grid connected plant with a governor.

The gain $\frac{S_{plant}}{S_{sys}}$ is used to convert from the plants base to the systems base. Plant model of hydro turbines will be elaborated in detail in Section 3.4.2.

3.3 Load sharing by multiple units

In this section, the contribution of multiple units to the power system and the corresponding equations that apply to this case are summarized. Figure 3.7 shows the block diagram of multiple units connected to the power system. The power is shared between the units according to the following formula

$$\frac{\Delta P_{m,i}}{\Delta P_{m,j}} = \frac{R_j}{R_i} \tag{3.6}$$

such that

$$\sum_{i=1}^{N} \Delta P_{m,i} = \Delta P_L + D\Delta\omega_r \tag{3.7}$$

where N is the number of units with speed-droop governor and i and j are integers indicating the unit index. Equation (3.6) only applies when the load set point (LSP) of the concerned units is equal to zero.

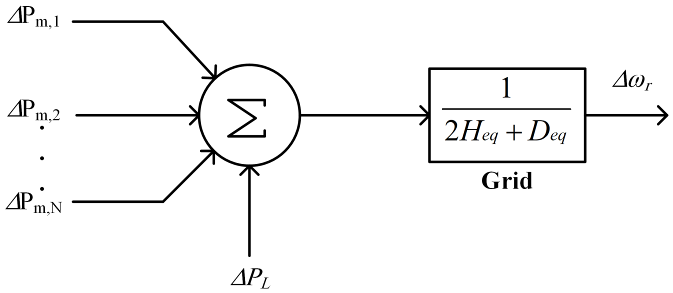

Figure 3.7: The block diagram of N number of units contributing to the power system.

Figure 3.8 shows graphically using the droop-speed characteristics how the power is shared among multiple units. If all the units are lumped into one unit, it would have an equivalent droop constant given by

$$\frac{1}{R_{eq}} = \frac{1}{R_1} + \frac{1}{R_2} + \cdots + \frac{1}{R_N} \tag{3.8}$$

If multiple subsystems are interconnected synchronously then the equivalent damping constant of the system is given by

$$D_{eq} = D_1 + D_2 + \cdots + D_M \tag{3.9}$$

where M is the number of subsystems connected synchronously. To extend (3.5) for multiple units, the steady state frequency deviation of the system is expressed as

$$\Delta\omega_{r,ss} = \frac{-\Delta P_L}{\frac{1}{R_{eq}} + D_{eq}} \tag{3.10}$$

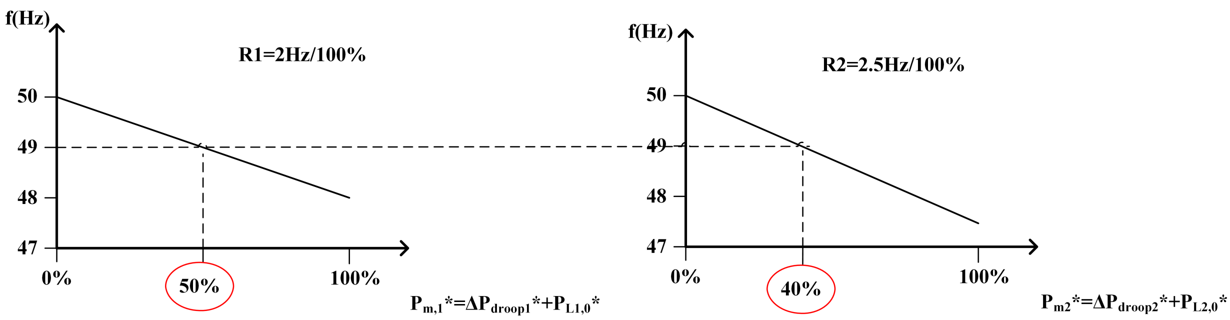

Figure 3.8: The droop-speed characteristics of two units with different droop constants showing the power share between them.

3.4 Hydro plant model

In this section, the hydro plant basic terminologies are explained and the mathematical model of the plant including the governor, actuator, penstock and the turbine are summarized.

3.4.1 Hydro plant terminologies

A typical hydro plant is shown in Figure 3.9. It consists of a reservoir from which the water is taken. The reservoir is at a higher elevation from the turbine in order for the water to gain kinetic energy while it is flowing downstream through the penstock. The difference in elevation between the reservoir and the turbine is called the head. Electricity is generated when the water hits the turbine and then it propagates through the transmission line to different consumers. The amount of generation is determined by the water rate of flow, which is controlled by the gate opening position.

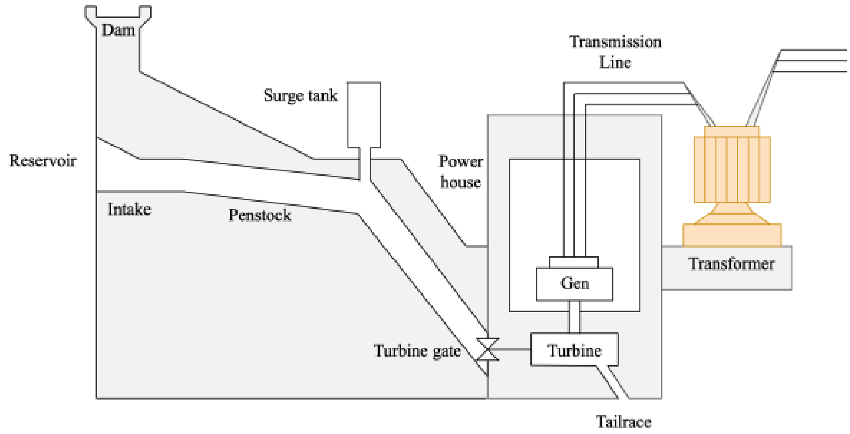

Figure 3.9: A basic hydro power station including reservoir, penstock, turbine, and generator grid interface [4].

There are many hydro turbine types and the installation of a certain type in a specific location depends on the geographical properties of that location. In this project our focus will be on Kaplan turbines which are commonly installed in Sweden in the NSA and have a low to medium head.

3.4.2 Mathematical model of hydro plants

The mathematical model of a hydro plant can vary in complexity depending on the accuracy of the model needed for the study. In this project, the linear model is considered to be sufficient for the studies. The linear model of the hydro turbine is shown in Figure 3.10. The governor is a PI-droop controller that determines the reference guide vane position to the actuator. The actuator is modeled with a first order transfer function with time delay T_y and a gain equal to 1 pu. In reality, the speed of gate opening is limited, thus, a rate limiter is added before the actuator to simulate this fact. The penstock and turbine are modeled by the composite transfer function

$$\frac{\Delta P_{\mathrm{m}}}{\Delta Y} = \frac{-T_{\mathrm{w}}Y_0 + 1}{0.5T_{\mathrm{w}}Y_0 + 1} \tag{3.11}$$

where ΔP_m is the FCR provision of the unit in pu of its own base, ΔY is the guide vane opening position in pu, Y_0 is the loading of the turbine in pu and T_w is the water time constant given in s [4]. The term $\frac{S_{\mathrm{hydro}}}{S_{\mathrm{sys}}}$ is to convert from the plants base to the systems base, where S_{hydro} is the online capacity of FCR providing units and S_{sys} is the online capacity of all generators in the NSA. S_{hydro} is calculated according to the following formula

$$S_{\mathrm{hydro}} = R.FCR^{\mathrm{max}}.\frac{\mathrm{f}_0}{\Delta f} \tag{3.12}$$

where FCR^{max} is the FCR capacity in the NSA, f_0 is the nominal frequency (50 Hz) and Δf is the maximum frequency deviation which is equal to 0.1 Hz (50-49.9) for FCR-N, and 0.4 Hz (49.9-49.5) for FCR-D. The limiter added after the governor is to indicate the maximum FCR capacity in the NSA. The external input can be used for secondary (aFRR) or tertiary frequency regulation (mFRR). This model of the hydro plant can be used for both FCR-N and FCR-D provision with the main difference is the deadband block distinguished with the dotted line. The function of this block is to activate the FCR-D at 49.9 Hz as indicated in the requirements, see Section 2.4.2.

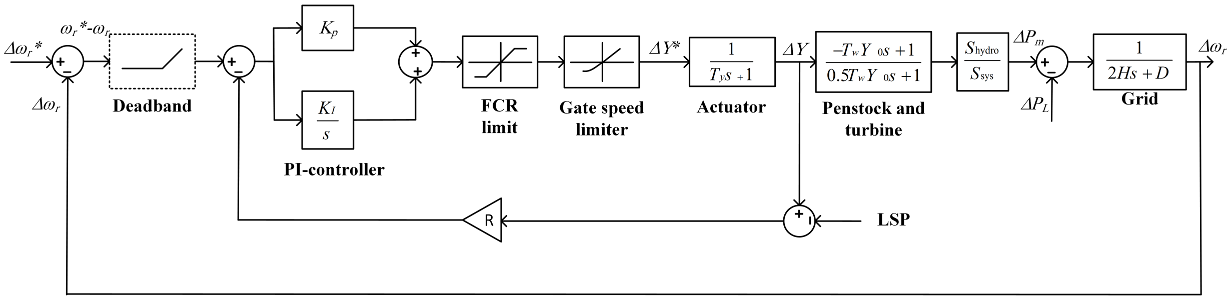

Figure 3.10: A block diagram of a linear hydro plant model. This model applies for both FCR-N and FCR-D except for the dashed deadband block which is only required for the FCR-D model.

In this project, the lumped hydro model is assumed to be a Kaplan model. Hence, it would have a Kaplan parameter values but with a capacity and FCR equivalent to that of the hydro turbines in the NSA. Table 3.1 shows typical Kaplan plant parameter, which will be used through out this project. There is a variety of governor settings that are used in the NSA. In this project, Vattenfall's settings listed in Table 3.2 are adopted. There are four main settings, EP0 till EP3. They differ mainly in the speed of response, determined by the PI controller parameters, and the droop characteristics, which indicates the amount of capacity at which the reserve is spread. According to (3.12), the higher the droop value, the more hydro capacity is involved in providing the reserve. Some providers use the same governor settings for both FCR-N and FCR-D, while others prefer using faster settings for FCR-D. However, different options are investigated in Section 6.2.

Table 3.1: Typical Kaplan plant parameters [4].

Symbol	Specifications	Value
T_{y}	Actuator time constant	0.2 s
T_{w}	Water time constant	1.6 s
Y_0	Unit loading	0.8 pu
U_{o}	Maximum gate opening speed	0.011 pu/s
U_{c}	Maximum gate closing speed	-0.011 pu/s

Table 3.2: Governor settings used in Vattenfall's turbines [15]

Parameter	EP0	EP1	EP2	EP3
E_{p}	0.1	0.04	0.02	0.01
K_{p}	1	1	1	2
K_{I}	1/6	5/12	5/6	5/6

3.4.3 Evaluation of wear and tear

Hydro turbines are subject to wear and tear due to their contribution in reserve provision especially during normal operation where they adjust their guide vane position continuously. A fundamental definition when discussing wear and tear is the accumulative movement distance of the guide vane. This can be evaluated by summing the distances travelled by the vane between each two direction changes. Figure 3.11 illustrates these fundamental concepts graphically.

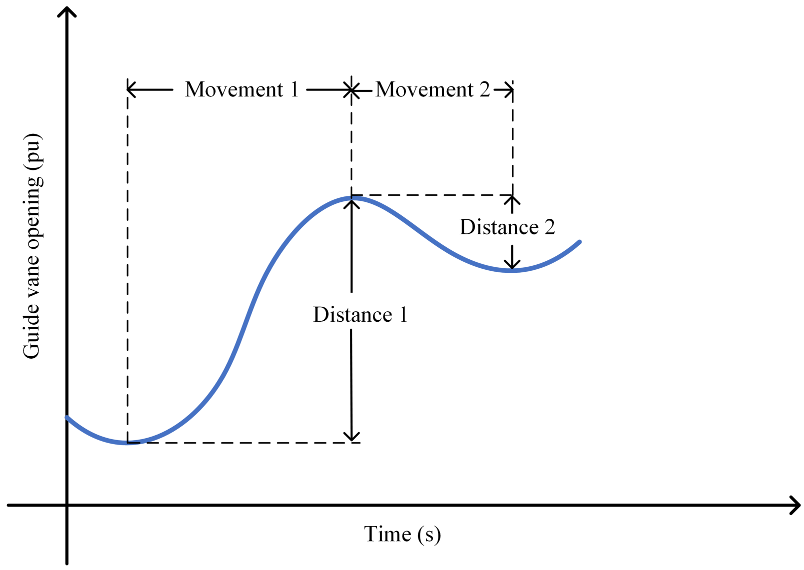

Figure 3.11: Guide vane movement and its distance.

The material deterioration can be evaluated using the following formula [18]

$$\omega_{\text{wear}} = K_{\text{wear}} P_{\text{Load}} D_y \tag{3.13}$$

where ω_{wear} is the linear wear in m, D_y is the accumulative distance movement in m, K_{wear} is the wear rate in m^2/N and P_{Load} is the specific load in N/m^2. Therefore, at a given load and wear rate constant, the linear wear of the material is linearly proportional to the travelled distance of the guide vane.

4

Modeling of VSWT for Dynamic Frequency Studies

In this chapter, the steady state characteristics and model of a GE 3.6 MW VSWT is summarized [5].

4.1 Steady state characteristics

The steady state characteristics of a WT include the rotor speed, extracted mechanical power and optimal pitch angle. In this section, these characteristics of the WT are plotted for MPPT operation. When the wind hits the blades of a WT, partial of that energy is converted into mechanical power that rotates the turbine, which is governed by

$$P_{\mathrm{mech}} = \frac{1}{2}\rho A C_{\mathrm{p}} V_{\mathrm{w}}^{3} \tag{4.1}$$

where P_{mech} is the mechanical power on the shaft of the turbine in W, ρ is the air density in $\mathrm{Kg/m^3}$, A is the rotor swept area in $\mathrm{m^2}$, C_{p} is the power coefficient and V_{w} is the wind speed in m/s. In this equation, all the parameters are specific for a given WT at a given site, except the power coefficient that can be controlled within a certain range. A mathematical representation of the power coefficient is given by

$$C_p(\beta,\lambda) = \sum_{i=0}^{4}\sum_{j=0}^{4} \alpha_{i,j}\beta^{i}\lambda^{j} \tag{4.2}$$

where $\alpha_{i,j}$ are constants that depend on the physical properties of the turbine, listed in Table 4.2, λ is the ratio between the tip speed of the blades and the wind speed, β is the pitch angle of the blades in degrees. Figure 4.1 shows a plot of the power coefficient with respect to tip-speed ratios ranging from 0 to 20 and different pitch angles. It is obvious that the power coefficient is higher for lower pitch angles and has an optimal tip-speed ratio for a given pitch angle at which the power coefficient becomes maximum. The maximum power coefficient that can be obtained is 0.5173 corresponding to a pitch angle equal to zero and an optimal tip-speed ratio equal to 8.8. The tip-speed ratio is obtained as

$$\lambda = \frac{\mathrm{K_b}\Omega_{\mathrm{r}}}{V_{\mathrm{w}}} \tag{4.3}$$

where $\mathrm{K_b}$ is a constant equivalent to the rotor radius in meters multiplied by the base angular speed of the rotor in rad/s, Ω_{r} is the rotor speed in pu and V_{w} is the wind speed in m/s. If the rotor speed is controlled to give the optimal tip-speed ratio for a given wind speed, then maximum power can be utilized.

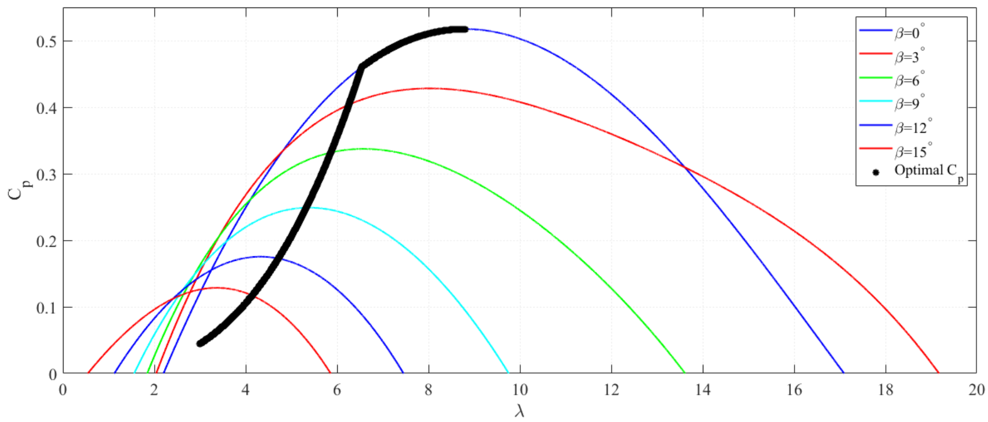

Figure 4.1: The power coefficient curve of the GE WT with respect to the tip-speed ratio and different pitch angles. The optimal C_p for MPPT operation is demonstrated by the black line.

According to the way in which a WT is operated, wind speeds are classified into three categories, low, medium and high wind speed ranges. During low wind speeds, the WT is being operated to follow the maximum power point (MPP). This is achieved by controlling the rotor speed to give $\lambda_{\text{opt}} = 8.8$ while keeping the pitch angle at minimum ($\beta = 0$) in order to get $C_{\text{p,max}} = 0.5173$. At medium wind speeds, the rotor speed would already hit the limits ($\Omega_{\text{r,max}} = 1.2pu$), thus, the MPPT control through rotor speed regulation is no longer possible as the rotor speed cannot be increased further when the wind speed continue to increase. As a result, the tip-speed ratio would decrease according to (4.3) and the operating point on the $C_\text{p} - \lambda$ curve will move to the left as shown by the black line in Figure 4.1. As the wind speed increases even more, the maximum power ratings of the turbine will be reached (P_{max} =1 pu). This range of speeds is called high wind speeds, during which the blades are pitched to spill the excess wind energy in order to not exceed the WT power limits. The instant at which the black line in Figure 4.1 leaves the blue curve is at which pitching is initiated. It is clear from the figure that the rate of decrease of the power coefficient is higher than that when it was following the blue curve. This is quite important since the mechanical power in (5.1) is proportional to the cubic of the wind speed, therefore, the power coefficient should be decreased faster in order to limit the mechanical power to 1 pu. Figure 4.2 shows a plot of the mechanical power, rotor speed and pitch angle for wind speeds in all the three ranges and corresponding to MPPT operation of the turbine. Notice that the power is zero for any wind speeds below 3 m/s (cut-in wind speed) and above 25 m/s (cut-out wind speed). Parameters of the turbine used for the calculations are shown in Table 4.1. The K_b value is not considered the same as in the GE report since it seems to be not updated. It is back calculated from the fact that the WT hits the maximum speed limits when the power is equal to 0.46 pu. From (4.1), the wind speed corresponding to that instant can be obtained and then substituted in (4.3) to obtain the K_b value. Notice that the C_{pmax} and λ_{opt} values are used for these calculations since we are still at the edge of the low wind speed range and thus they are feasible.

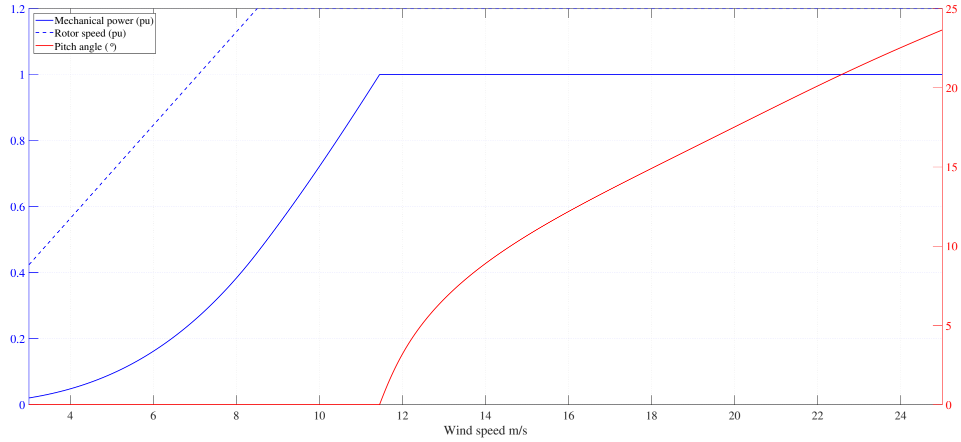

Figure 4.2: Mechanical power, rotor speed and pitch angle of the GE turbine corresponding to MPPT operation at different wind speed ranges.

Table 4.1: GE 3.6 MW WT parameters

Parameter	value
$\frac{\frac{1}{2}\rho A_r}{S_b}$	0.00145 pu
K_b	62.3386

According to the previous discussion, the controlled parameter of the WT in order to achieve maximum power operation is the rotor speed. The question is, at a certain time instant when the wind speed is constant, what is the optimal rotor speed that gives MPPT? To answer this question the mechanical power is plotted against the rotor speed for different wind speeds as shown in Figure 4.3. The plot follows the same trend as in Figure 4.1 where there is only one point in the graph at which the maximum power is obtained. A line that connects all these points is called an MPPT line and is clarified by the black dotted line in the same figure. This line is important as will be seen in the next section to obtain the optimal reference rotor speed for the controller.

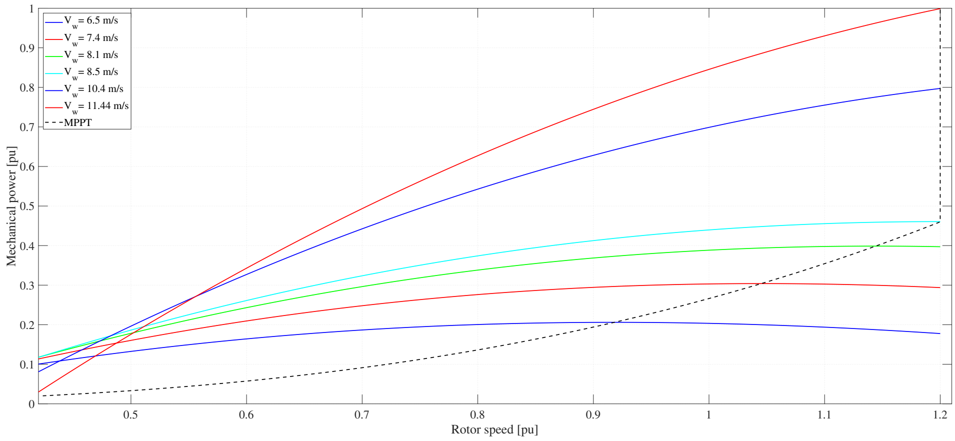

Figure 4.3: A plot of the mechanical power against the rotor speed for different wind speeds. The MPPT operation of the turbine is denoted by the dotted line.

Table 4.2: C_p coefficients.

i	j	$\alpha_{i,j}$
	j=0	$-4.1909\times10^{-}1$
	j=1	$2.1808\times10^{-}1$
i=0	j=2	$-1.2406\times10^{-}2$
	j=3	$-1.3365\times10^{-}4$
	j=4	$1.1524\times10^{-}5$
	j=0	$-6.7606\times10^{-}2$
	j=1	$6.0405\times10^{-}2$
i=1	j=2	$-1.3934\times10^{-}2$
	j=3	$1.0683\times10^{-}3$
	j=4	$-2.3895\times10^{-}5$
	j=0	$1.5727\times10^{-}2$
	j=1	$-1.0996\times10^{-}2$
i=2	j=2	$2.1495\times10^{-}3$
	j=3	$-1.4855\times10^{-}4$
	j=4	$2.7937\times10^{-}6$
	j=0	$-8.6018\times10^{-}4$
	j=1	$5.7051\times10^{-}4$
i=3	j=2	$-1.0479\times10^{-}4$
	j=3	$5.9924\times10^{-}6$
	j=4	$-8.9194\times10^{-}8$
	j=0	$1.4787\times10^{-}5$
	j=1	$-9.4839\times10^{-}6$
i=4	j=2	$1.6167\times10^{-}6$
	j=3	$-7.1535\times10^{-}8$
	j=4	$4.9686\times10^{-}10$

4.2 VSWT model and control

The block diagram of the GE 3.6 MW VSWT is summarized in this section, where the objective is to achieve the MPPT operation described in the previous section. Figure 4.4 shows the block diagram of such a VSWT and its control. The input to the model is the wind speed, where it goes to a block that calculates the mechanical power extracted from wind similar to (4.1). Then the one mass rotor model, which is basically the swing equation, is used to calculate the rotor speed. After that, the electrical power required for the rotor speed to follow the reference is computed using a speed controller. The reference rotor speed is determined based on the MPPT curve in Figure 4.3. Before that, a low pass filter is applied on the measured electrical power to remove the noise. Finally, during the high speed range, the pitch angle controller is activated when the electrical power hits the limit. It determines the pitch angle necessary to keep the mechanical power at 1 pu. Notice that in the pitch control the mechanical power is controlled so that the electrical power output is limited to 1 pu. In contrast, during the low wind speed range, the speed controller controls the electrical power to follow changes in mechanical power. The inertia emulation block is not an essential part for the operation of any WT but rather an optional choice. During normal operation this block is disabled but when there is a disturbance in the system (under-frequency), it is activated to provide temporary extra power support to the grid. However, when providing frequency support, the rotor speed might drop a lot, which might cause the torque to exceed its limits. Therefore, there is an essential need for a torque limiter to ensure that the limits are not exceeded. The reference power recalculated by the torque limiter becomes an input to the power converter which injects this power into the grid. The output of the VSWT block must be converted to the system's base when the model is used as a part of a power system. This is done, similar to the hydro model, by multiplying the output with the unit's online capacity (S_{bw}) and dividing by the online capacity of the power system (S_{b}).

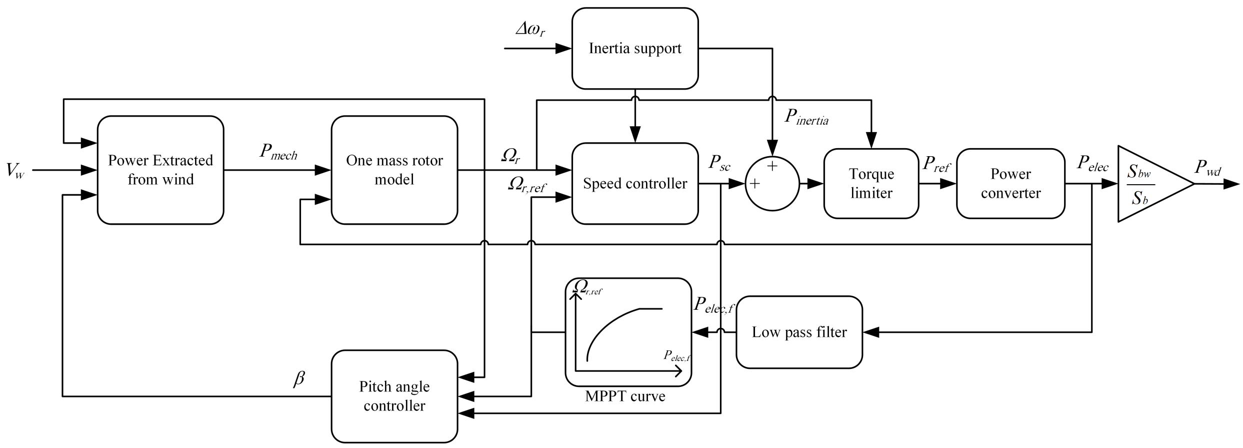

Figure 4.4: VSWT block diagram model.

4.2.1 Power extracted from wind model

Figure 4.5 shows the block diagram used to calculate the power extracted from the wind. The inputs to the model are the rotor speed, wind speed and the pitch angle. Using (4.3), the tip-speed ratio is calculated, and along with the pitch angle, the power coefficient is determined according to (4.2). Finally the mechanical power is obtained according to (4.1).

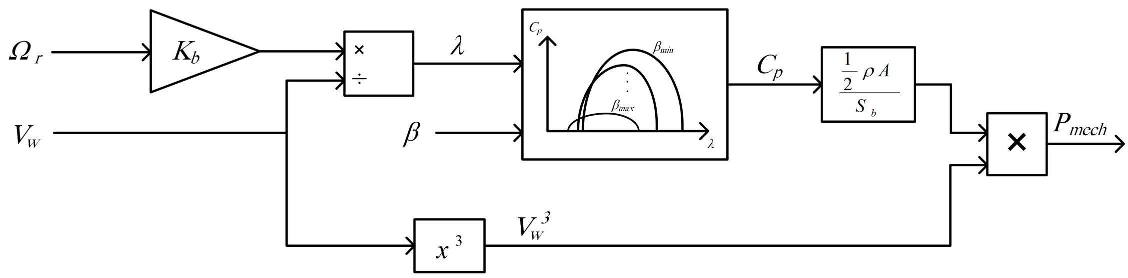

Figure 4.5: Power extracted from wind block diagram model.

4.2.2 One mass rotor model

The one mass rotor model is the physical representation of the turbine and the generator as a one mass that has an inertia constant of 5.74 s. The block diagram of the model is shown in Figure 4.6. This model is a representation of the swing equation (2.3) in the s-domain, where the mechanical power and the electrical power are the inputs, and the rotor speed is the output.

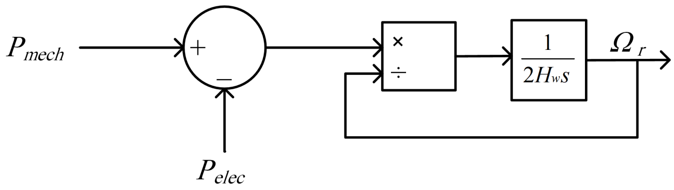

Figure 4.6: One mass rotor model block diagram.

4.2.3 Speed controller

The block diagram of the speed controller is shown in Figure 4.7. It has the functionality of controlling the rotor speed to follow an optimal reference speed that governs the MPPT operation of the turbine. This control action is achieved by computing the reference electrical power to be injected into the grid. A saturation block is added so that the power limits of the turbine are not exceeded. To avoid overcharging of the integrator an antiwindup is inserted to the input of the integral part of the controller. Table 4.3 shows the parameters used for the speed controller.

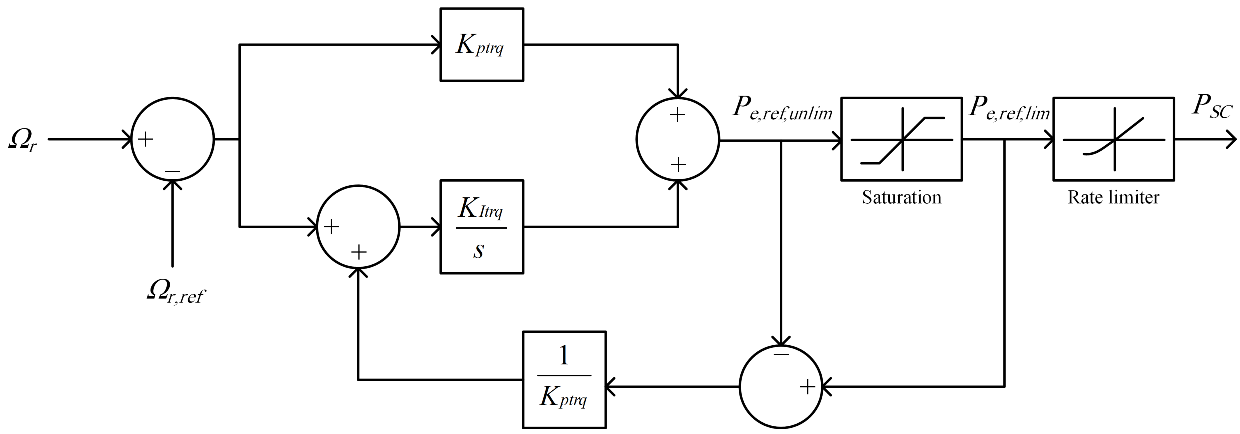

Figure 4.7: Block diagram of the speed controller.

Table 4.3: Speed control parameters.

Parameter	**Value**
K_{ptrq}	3 [5]
K_{Itrq}	0.6 [5]
P_{max}	1 pu
P_{min}	0 pu
dp_{max}/dt	0.45 pu/s [5]
dp_{min}/dt	-0.45 pu/s [5]
T_{filter}	5 s

4.2.4 Torque limiter and power converter

Figure 4.8 shows the torque limiter and the power converter models. The reference power coming from both the speed controller and the inertia support blocks is first divided by the rotor speed in order to obtain the reference torque. Then, the torque is limited to its maximum value ($\frac{P_{max}}{\Omega_{max}}$) in case the reference exceeds that. After that, the reference power is calculated again by multiplying the limited torque with the rotor speed. The reference power is then divided by the terminal voltage in order to calculate the reference current for the power converter. The converter time constant block is a representation of the time needed by the converter to inject this amount of reference power to the grid. Parameters used in these block diagrams are listed in Table 4.4.

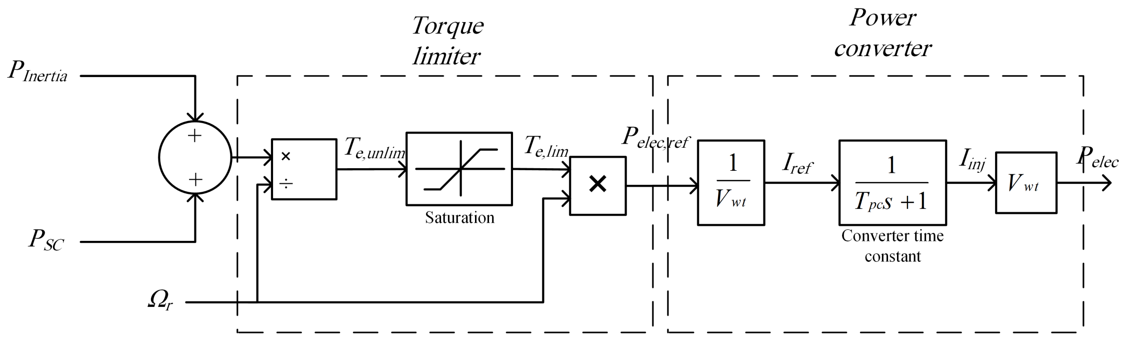

Figure 4.8: Converter time constant representing the time constant of active power response.

Table 4.4: Torque limiter and power converter parameters.

Parameter	Value
T_{max}	0.83 pu
T_{min}	0 pu
V_{wt}	1 pu
T_{pc}	0.05 s [5]

4.2.5 Pitch angle controller

The pitch angle controller block diagram, as shown in Figure 4.9, consists of two controllers, a pitch control and a pitch compensation. During low and medium wind speeds where the maximum power limit is not yet exceeded, the pitch control is not activated. Thus, the pitch compensation is needed to compensate for the output of pitch control during these wind speeds. The input to the pitch compensation is the speed controller's electrical power minus the maximum electrical power. During high wind speeds, the electrical power is equal to the maximum, thus, the pitch compensation is disabled, allowing the pitch controller to function normally. Any step increase in wind speed will cause the rotor to accelerate and is sensed by the pitch control as positive input ($\omega_{\mathrm{r}} > \omega_{\mathrm{r,ref}}$), hence, an increase in the pitch angle is expected. The saturation and rate limiter blocks are there to ensure that the physical limits of the blade pitch are not exceeded. An antiwindup is necessary in this situation on pitch angle limits for both controllers to avoid overcharging of integral controllers. The blade pitch time constant is a reflection of the time needed by the motor to pitch the blades. Table 4.5 shows the parameters used for the pitch angle controller.

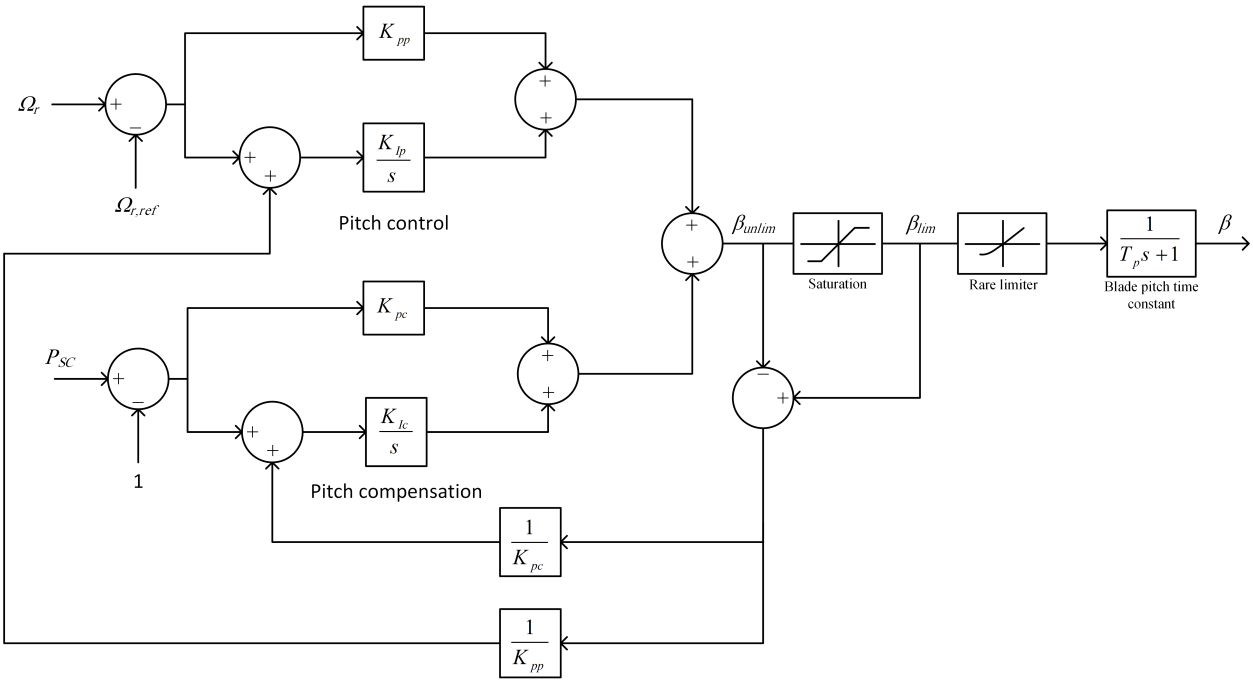

Figure 4.9: Pitch angle controller block diagram.

Table 4.5: Pitch angle controller parameters [5].

Parameter	Value
K_{pp}	150
K_{Ip}	25
K_{pc}	3
K_{Ic}	30
β_{max}	27 deg
β_{min}	0 deg
$d\beta_{max}/dt$	10 deg/s
$d\beta_{min}/dt$	-10 deg/s
T_p	0.3 s

4.2.6 Inertia emulator

The inertia emulation block is intended to emulate the response of a conventional generator during a disturbance. This means that the output power of this block should be proportional to the inverse of the RoCoF. This extra energy comes from the rotor's kinetic energy during low and medium wind speeds (assuming fixed wind speed). Thus, the speed controller should be relaxed in order to allow the speed to fall freely. This is done by coordination between the speed controller and the inertia emulation block diagrams such that the proportional and integral gains of the speed controller are changed to 0.5 and 0.05, respectively, as soon as the frequency support starts. During high wind speeds, most of the energy comes from down-regulating the pitch angle, since the pitch controller is not disabled. Figure 4.10 shows the detailed model of the inertia emulation block diagram. The input to this block is the inverse of the frequency deviation. Inertia is enabled when the frequency falls below a pre-determined activation frequency ($\Delta\omega_{r,act}$). The frequency signal is then filtered from noise using a low pass filter. Analogous to the swing equation, the $2H_{syn}$ gain here represents the synthetic inertia constant. Following that, a high pass filter with time constant T_{hp} is applied. This can be imagined as a differentiator ($T_{hp}s$) cascaded with a low pass filter ($\frac{1}{T_{hp}s+1}$) to filter the signal resulting from differentiation. Finally, the output power is limited with a saturation and a rate limiter blocks. The purpose of these might be physical limits (e.g. converter's rated power or rated rate of change of power) or other requirements (e.g. grid codes). Parameters used in this block are presented in Table 4.6.

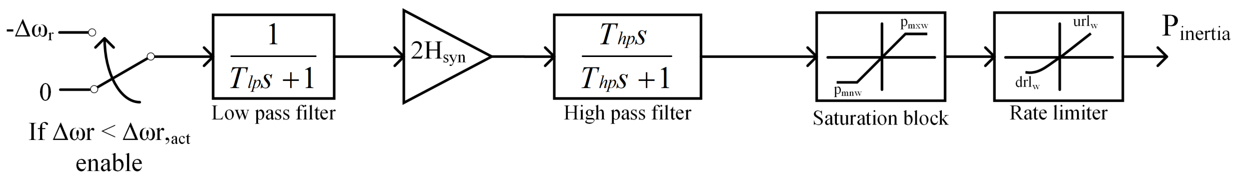

Figure 4.10: Inertia emulation block diagram

Table 4.6: Inertia emulation block parameters [5].

Variable	Value
T_{lp}	1 s
T_{hp}	5.5 s
P_{max}	0.1 pu
P_{min}	0 pu
url_w	0.1 pu/s
drl_w	-1.0 pu/s

5

Generation Scenarios and Inertia Estimation

In this chapter, the inertia of the NSA in a windy summer day of 2040 is estimated. A summer season in the NSA has the lowest load among other seasons of the year. Hydro units are responsible for adjusting their power to compensate for wind power variations. Therefore, a windy summer scenario constitutes a case where the inertia of the system is the lowest through out the year.

5.1 Generation estimation methods

In this section, two methods are developed to estimate the generation in 2040. One of them considers the wind power proportional to the installed capacity (inelastic wind power), while in the other method the wind power is adjusted to meet the demand (elastic wind power). This does not imply the curtailment of wind power, but rather just to generate a different scenario that can be interesting.

5.1.1 Elastic wind power method

In the elastic wind power (EWP) method, the generation in 2040 is assumed equal to the generation in 2019 multiplied by the installed capacity ratio between 2040 and 2019. This product is then multiplied with a scaling factor to provide flexibility in the generation in order to meet the demand. In this case, all generation technologies including wind tribunes are provided with a scaling factor to adjust their generation. However, this does not mean curtailing wind power. The mathematical representation of this method is given by

$$P_{11_{2040}} = xP_{11_{2019}} \frac{CP_{11_{2040}}}{CP_{11_{2019}}} \tag{5.1}$$

$$P_{12_{2040}} = xP_{12_{2019}} \frac{CP_{12_{2040}}}{CP_{12_{2019}}} \tag{5.2}$$

$$\vdots$$

$$P_{mn_{2040}} = xP_{mn_{2019}} \frac{CP_{mn_{2040}}}{CP_{mn_{2019}}} \tag{5.3}$$

where P_{2019} is the actual power generation in 2019, P_{2040} is the estimated power generation in 2040, CP_{2019} is the actual installed capacity in 2019, CP_{2040} is the estimated installed capacity in 2040, m is an index indicating the number of generation technologies, n is an index indicating the number of countries and x is a scaling factor used to match the load with the generation. By knowing that the load is expected to increase by 15% in 2040 [11], and assuming that the net export will also rise by 15% as well, the scaling factor x can be found using the following power balance equation

$$x\sum_{i=1}^{m}\sum_{j=1}^{n} P_{ij_{2019}} \frac{CP_{ij_{2040}}}{CP_{ij_{2019}}} = 1.15(P_{\text{load}_{2019}} + P_{\text{Ex}_{2019}}) \tag{5.4}$$

where $P_{\text{load}_{2019}}$ is the load in 2019 and $P_{\text{Ex}_{2019}}$ is the power exchange in 2019. By back substituting the factor x in Equations (5.1) through (5.3), the estimated power generation in 2040 is found.

5.1.2 Inelastic wind power method

In contrast to the previous method, the wind power is not multiplied by the scaling factor in the inelastic wind power (IWP) method. This makes the wind power proportional to the installed capacity increase between the periods 2019 and 2040 under the assumption that the wind speed is the same and no geographical smoothing. This is expressed in equations as

$$P_{11_{2040}} = xP_{11_{2019}} \frac{CP_{11_{2040}}}{CP_{11_{2019}}} \tag{5.5}$$

$$P_{12_{2040}} = xP_{12_{2019}} \frac{CP_{12_{2040}}}{CP_{12_{2019}}} \tag{5.6}$$

$$\vdots$$

$$P_{mn_{2040}} = xP_{mn_{2019}} \frac{CP_{mn_{2040}}}{CP_{mn_{2019}}} \tag{5.7}$$

$$P_{\text{wd}1_{2040}} = P_{\text{wd}1_{2019}} \frac{CP_{\text{wd}1_{2040}}}{CP_{\text{wd}1_{2019}}} \tag{5.8}$$

$$P_{\text{wd}2_{2040}} = P_{\text{wd}2_{2019}} \frac{CP_{\text{wd}2_{2040}}}{CP_{\text{wd}2_{2019}}} \tag{5.9}$$

$$\vdots$$

$$P_{\text{wd}n_{2040}} = P_{\text{wd}n_{2019}} \frac{CP_{\text{wd}n_{2040}}}{CP_{\text{wd}n_{2019}}} \tag{5.10}$$

where m is an index indicating the number of generation technologies excluding wind power. The factor x can be found using the following equation

$$\sum_{j=1}^{n} P_{\text{wd}j_{2019}} \frac{CP_{\text{wd}j_{2040}}}{CP_{\text{wd}j_{2019}}} + x\sum_{i=1}^{m}\sum_{j=1}^{n} P_{ij_{2019}} \frac{CP_{ij_{2040}}}{CP_{ij_{2019}}} = 1.15(P_{\text{load}_{2019}} + P_{\text{Ex}_{2019}}) \tag{5.11}$$

5.2 Nordic Grid Development Plan

5.2.1 Generation capacity mix estimation by SvK

The Nordic Grid Development Plan (NGDP) is published every second year with the latest in 2019 [11]. The purpose is to evaluate a future view on the Nordic grid, predict problems that might arise and plan early for them. The report contains scenarios of the installed capacity of different types of generation in the Nordic countries in 2040, with the best estimate one called the reference scenario (RS). Installed capacity in the Nordic countries in 2019 by type can be found in ENTSO-E's transparency platform [10] and is demonstrated in Figure 5.1 (left). There are five main resources of electricity in the Nordic countries, hydro, nuclear, wind, biomass and fossil fuel. The NGDP-RS of installed capacities in 2040 is illustrated in Figure 5.1 (right). The NGDP predicts no change in the current hydro installed capacity except for small hydro projects of about 5 GW in Norway as shown in Figure 5.1. Biomass is assumed as well to be quite stable between the years 2019 and 2040. Nuclear power in Sweden is decommissioned completely by 2040, while in Finland some nuclear power is left due to the commissioning of new nuclear power stations, Olkiluoto 3 with a net capacity of 1600 MW and expected commissioning date 2021, and Hanikivi with a net capacity of 1200 MW and expected commissioning date 2028 [14]. Fossil fuel capacity is expected to reduce a lot by 2040 due to its CO_2 emissions and will be present only as natural gas. Wind power will increase dramatically to compensate for the energy production loss due to the decommissioning of nuclear and fossil fuel units.

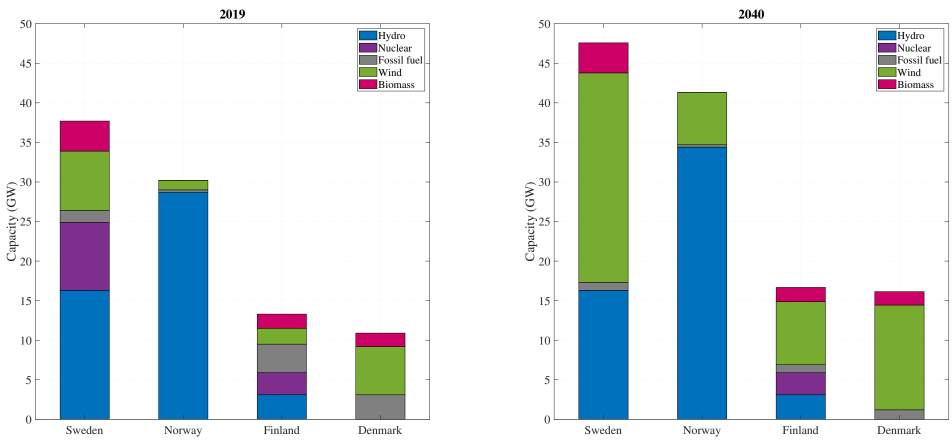

Figure 5.1: Actual installed capacity in the Nordic countries in 2019 (left) and the NGDP-RS for the installed capacity in 2040 (right).

Due to the lack of information some assumptions are made. The biomass installed capacity in Sweden in 2019 is not available in the ENTSO-E's transparency platform. Thus, it is assumed equal to that in the ENTSO-E'S Ten Year Network Development plan (TYNDP) of 2020 [13]. Furthermore, the fossil fuel generation of 2019 is back estimated from that of 2020 in [11] using the same slope. That is done for consistency with the NGDP-RS, because there is a great variety of fossil fuel resources in the transparency platform that might lead to inconsistency due to their large capacity if added all. It is also important to note that in [11] the wind energy is expressed in TWh per year specified for each Nordic country. Moreover, in [12] the total installed wind capacity in the Nordic countries in 2040 is presented. By combining these two information the average capacity factor of a wind turbine is determined and therefore the wind capacity per country can be back calculated. Furthermore, the small hydro projects were not mentioned quantitatively in [11], so again based on the total hydro capacity in the Nordic countries in [12], and by assuming constant hydro power in other countries, the capacity of hydro power in Norway in 2040 is obtained. It is worth mentioning also that other types of generation with insignificant amount of capacity are discarded from this study, e.g., waste and other renewable.

5.2.2 Elastic wind power scenario

In this section, the generation in the NSA in 2040 is estimated based on the NGDP-RS and using the methods demonstrated in Section 5.1. A windy summer scenario is picked up from ENTSO-E's transparency platform, which is the 1st of July 2019, 00:01 CET, Monday. Figure 5.2 shows the actual generation by country and technology at that particular time (left) and the estimated generation in 2040 (right). It is noticed that Sweden has the highest amount of generation at that particular hour with roughly 16 GWh/h distributed between hydro, nuclear and wind. Norway comes in the second place with approximately 10 GWh/h coming mostly from hydro. Finland has the greatest variety of energy resources summing totally to around 6 GWh/h. Lastly comes Denmark market area 2 (DK2), which provides almost all of its generation from wind summing roughly to 0.5 GWh/h. The most attracting trend in 2040, is that all Nordic countries have much higher amount of wind energy. Another noticeable difference is that Sweden has phased out its nuclear energy.

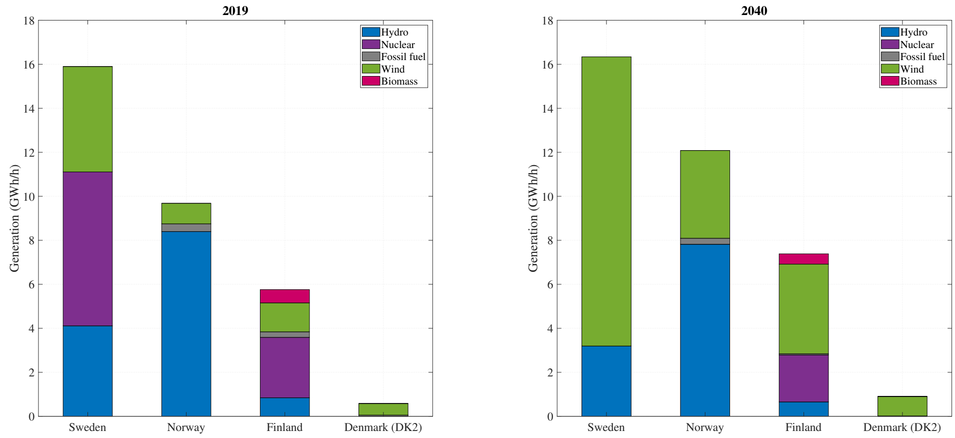

Figure 5.2: Actual generation in the NSA corresponding to the 1st of July 2019, 00:01 CET, Monday (left), and the estimated generation in 2040 corresponding to the NGDP-RS and using the EWP method (right).

Figure 5.3 shows the corresponding load and the net export at that particular hour. It can be seen that the load is quite low, roughly 30 GWh/h, which is a normal case during a summer night. The net export is calculated by subtracting the load from the total generation and it appears to be positive, which might be attributed to the excessive wind generation and cheaper electricity price in the NSA. The load and export in 2040 are assumed to increase by 15% as discussed in Section 5.1.1. Nevertheless, it is difficult to predict the net export in 2040 because it depends on other synchronous areas and the net export capacity as well.

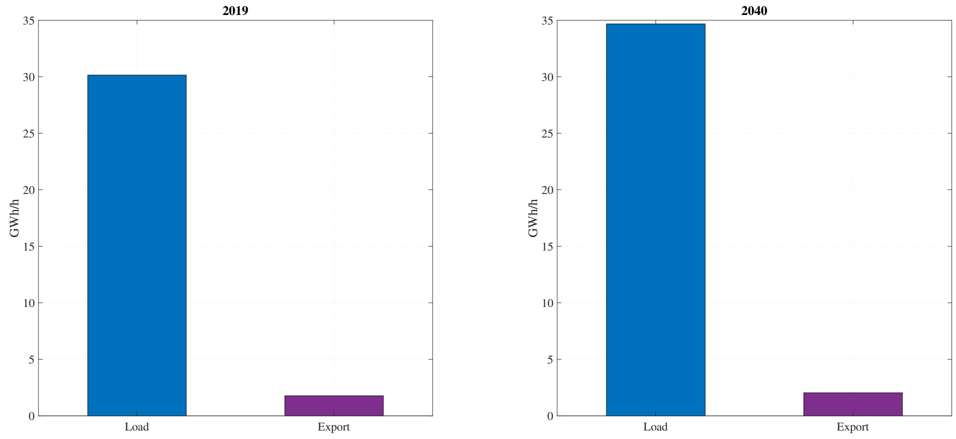

Figure 5.3: Actual load and net export in the NSA in 2019 corresponding to the 1st of July 2019, 00:01 CET, Monday (left), and the estimated load and net export in 2040 (right).

Figure 5.4 shows the penetration level of each type of generation in the NSA. It is obvious that the wind penetration level is quite high at that period of time (24%), but still the hydro power provides the greatest amount of energy (42%), and the nuclear in the second place (31%). Figure 5.2 (right) is obtained by applying the EWP method. As expected, the wind penetration level has significantly increased to 60% because it has the highest capacity ratio among other types of generation. Nuclear is reduced dramatically dropping to 6% nuclear energy share in 2040. The other generation types have relatively minor changes.

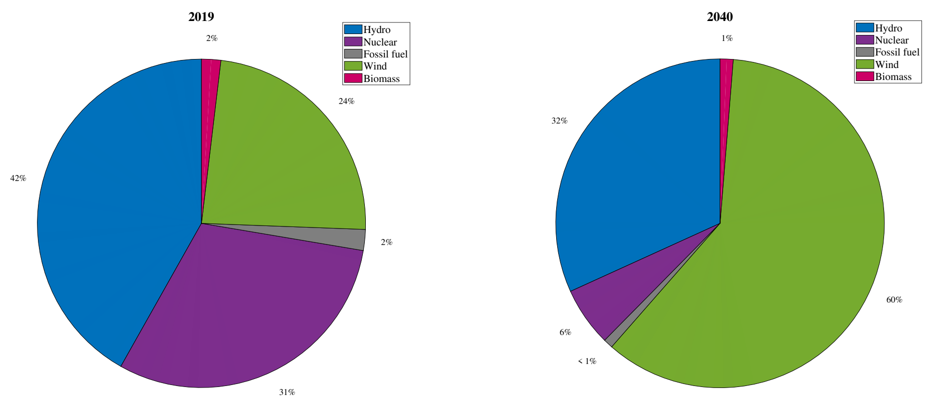

Figure 5.4: Penetration levels of different types of generation corresponding to those in Figure 5.2.

5.2.3 Inelastic wind power scenario

Figure 5.5 shows the generation in 2040 using the IWP method, while the corresponding penetration level in hundred percents is illustrated in Figure 5.6. It is obvious from the first glance that wind penetration levels have increased incredibly in 2040 compared to the EWP method. This is actually decided by the scaling factor in the EWP method, if it is less than one, then wind energy is expected to increase, and vice versa. It makes more sense when realising that the scaling factor in the elastic method is 0.78, which gives a great margin of increase for the wind energy. This is clearly shown in the wind penetration level which has increased to 77% in 2040.

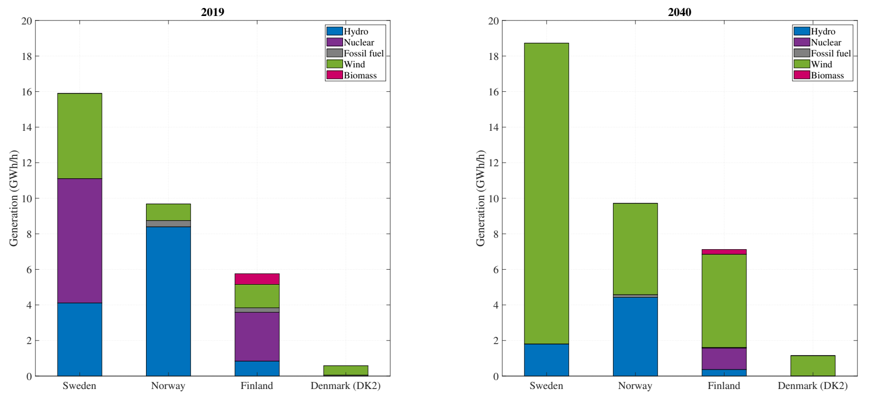

Figure 5.5: Actual generation in the NSA corresponding to the 1st of July 2019, 00:01 CET, Monday (left), and the estimated generation in 2040 corresponding to the NGDP-RS and using the IWP method (right).

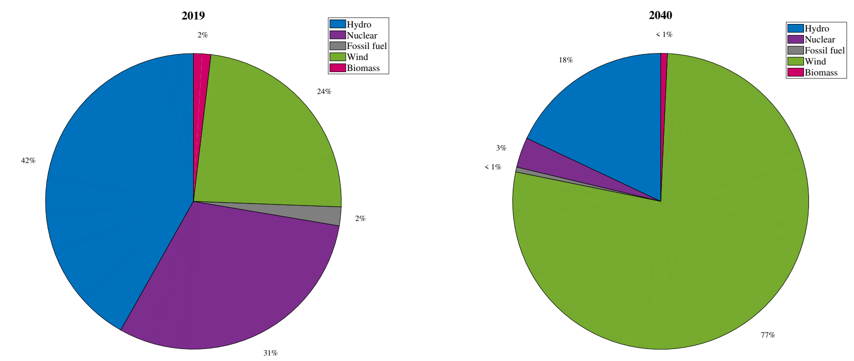

Figure 5.6: Penetration levels of different types of generation corresponding to those in Figure 5.5.

5.3 Ten Year Network Development plan

5.3.1 Generation capacity mix by ENTSO-E

The TYNDP is published every two years by ENTSO-E. It is similar to the NGDP but on the European level. The scenario that will be considered in this report is called the sustainable transition (ST), which is equivalent to the RS in the NGDP but has less degree of detail at the Nordic level in particular. The TYNDP-ST scenario for the Nordic countries in 2040 is presented in Figure 5.7 [13]. The most remarkable difference between TYNDP-ST and NGDP-RS is that the nuclear power in Sweden is not decommissioned completely in 2040. Furthermore, wind power is dramatically increased by 2040 but on a slower pace than in the NGDP. However, hydro power has less uncertainty with both reports predicting that only slight increase in the capacity in Norway is expected to occur. Biomass is considered to stay roughly the same in Sweden, almost doubles in Finland, and decreases by half in Denmark, but overall it is quite stable. The total fossil fuel has been reduced and is anticipated to consist of only natural gas in 2040. Overall, the trend towards renewable energy has been assumed to go faster in the NGDP-RS than in TYNDP-ST.

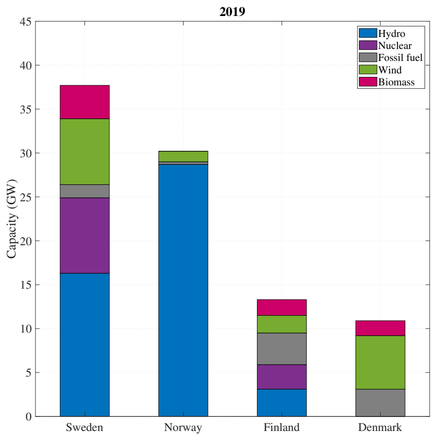

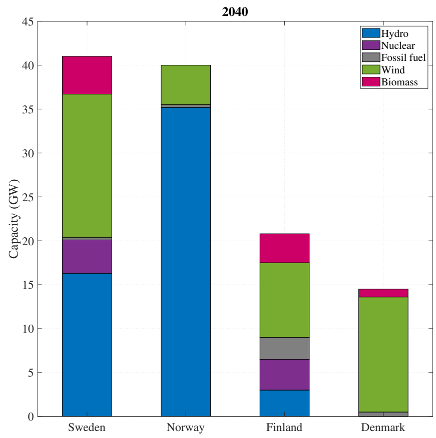

Figure 5.7: Actual installed capacity in the Nordic countries in 2019 (left) and the TYNDP-ST scenario for the installed capacity in 2040 (right).

5.3.2 Elastic wind power scenario

The generation in 2040 corresponding to the elastic wind power scenario is illustrated in Figure 5.8, while the corresponding penetration levels by technology is shown in Figure 5.9. It is noticed that wind power has the highest share of energy (47 %) at that hour but with lower penetration level than in the NGDP case. Another remarkable difference is that synchronous based generation has the highest share of energy coming mostly from hydro (35%) and nuclear (15%). Also, it can be seen that Sweden has lower share of energy in

2040 than in 2019 even though the load is increasing. Nevertheless, Finland and Norway are providing much more energy in 2040, covering the gap of Sweden's energy reduction.

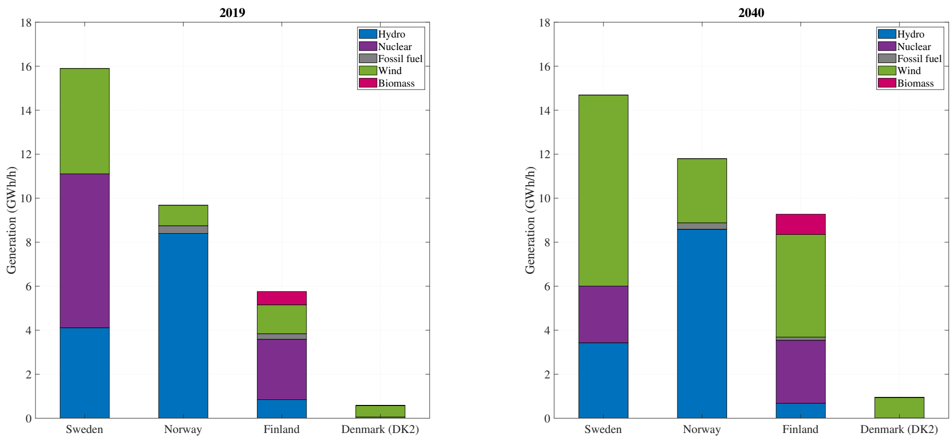

Figure 5.8: Actual generation in the NSA corresponding to the 1st of July 2019, 00:01 CET, Monday (left), and the estimated generation in 2040 corresponding to the TYNDP-ST scenario and using the EWP method (right).

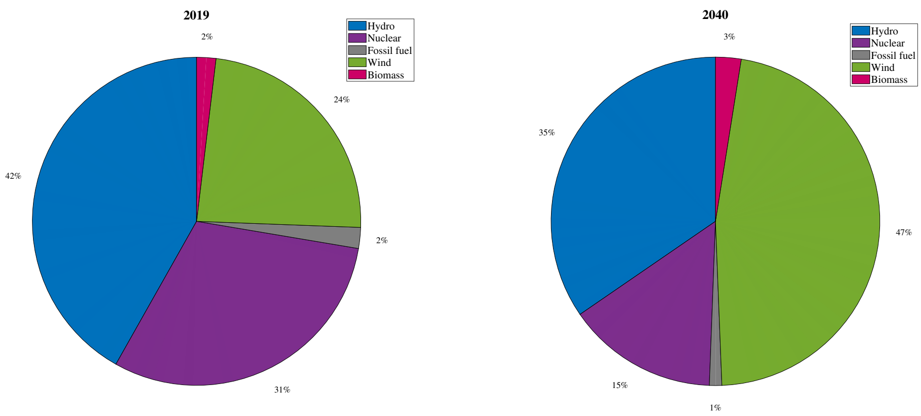

Figure 5.9: Penetration levels of different types of generation corresponding to those in Figure 5.8.

5.3.3 Inelastic wind power scenario

Figures 5.10 and 5.11 show the generation in 2040 corresponding to the inelastic wind power method and the share of energy by type, respectively. The main dissimilarities with elastic method is that non-synchronous based generation has the highest share of energy with wind energy rising to 56%.

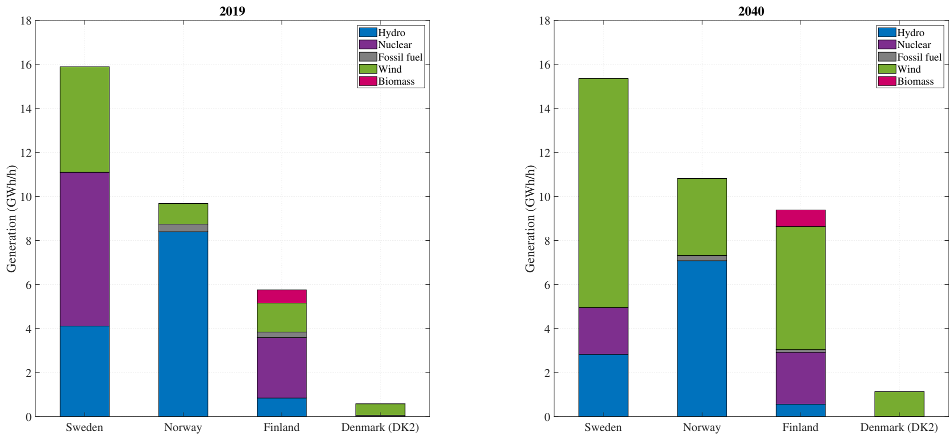

Figure 5.10: Actual generation in the NSA corresponding to the 1st of July 2019, 00:01 CET, Monday (left), and the estimated generation in 2040 corresponding to the TYNDP-ST scenario and using the IWP method (right).

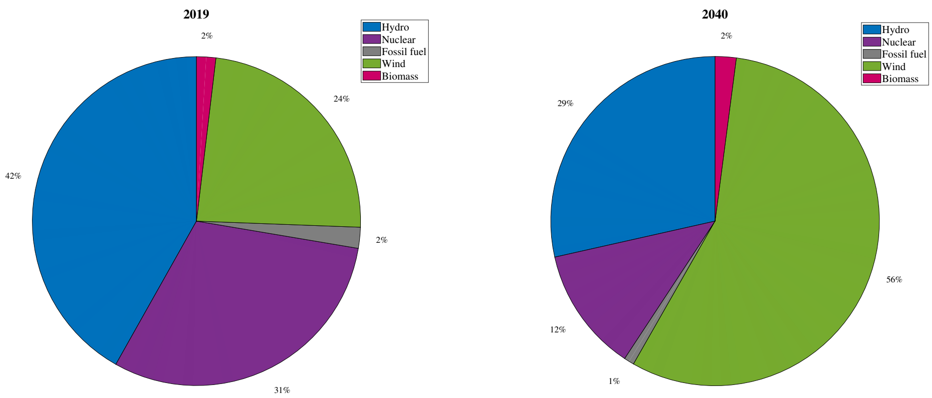

Figure 5.11: Penetration levels of different types of generation corresponding to those in Figure 5.10.

5.4 Inertia estimation

Now, by knowing the generation in 2040 using either the elastic or inelastic wind power methods, the online capacity can be determined as

$$S_{\mathrm{b}} = \sum_{i=1}^{m}\sum_{j=1}^{n} \frac{P_{\mathrm{G_{ij}}}}{PF_i L_i} \tag{5.12}$$

where PF is the power factor of the unit and L is its loading. Table 5.1 lists the power factors and loading of different unit types used for the calculation of the online power capacity.

Table 5.1: Typical power factors and loading of different generation types.

Unit type	Power factor	Loading
Hydro	0.9 [4]	0.8 [4]
Nuclear	0.9 [4]	1 [4]
Thermal	0.9 [4]	1 [4]
Wind	1 [4]	1 [4]
Biomass	0.9	1

The rotational kinetic energy stored in the NSA is calculated as

$$E_{\mathrm{K}} = \sum_{i=1}^{m}\sum_{j=1}^{n} H_{ij} S_{ij} \tag{5.13}$$

where H is the inertia constant of the generating unit and S is its online power capacity. The different inertia constants of the generating units in the Nordic countries are shown in Table 5.2. While biomass is assumed to have the same inertia constant as thermal units in each respective country.

Table 5.2: Typical inertia constants of different types of generation in each Nordic country [4].

Unit type \ Country	Sweden	Norway	Finland	Denmark
Hydro	4.5	2.9	2.8	-
Nuclear	6.2	-	6.6	-
Thermal	2.9	2.5	4.4	4.5
Wind	0	0	0	0

After determining the Online capacity and the kinetic energy in the NSA, the equivalent inertia constant is calculated as

$$H_{\mathrm{eq}} = \frac{E_{\mathrm{K}}}{S_{\mathrm{b}}} \tag{5.14}$$

The load-frequency damping constant of the NSA is assumed equal to 400 MW/Hz. This value is converted to pu as

$$D_{\text{pu}} = D_{\text{actual}} \frac{f_{\text{b}}}{S_{\text{b}}} \tag{5.15}$$

Table 5.3 shows the calculated parameters of the NSA in 2019 and the estimated values for 2040. It is clear that the inertia has dropped significantly between the years 2019 and 2040. This is mostly due to the increase of the wind penetration levels, which does not contribute to inertial support due to power-electronic converters. Additionally, the decommissioning of large synchronous generators in the system, especially nuclear and thermal units, led to the loss of a massive rotating kinetic energy in the system. In general, the total kinetic energy in the system and the inertia constant tend to decrease with higher wind penetration levels.

Table 5.3: Calculated power system parameters corresponding to the 1st of July 2019, 00:01 CET, Monday, and the estimated parameters in 2040 using different scenarios.

	H (s)	D (pu)	S_{b} (GVA)	KE (GWs)	Wind penetration level (%)
2019	3.56	0.52	38.3	136.6	24%
NGDP-RS-EWP 2040	1.76	0.48	41.6	73	60%
NGDP-RS-IWP 2040	1.05	0.51	39.5	41.3	77%
TYNDP-ST-EWP 2040	2.44	0.47	42.4	103.5	47%
TYNDP-ST-IWP 2040	2.06	0.48	41.4	85.3	56%

6

Case Studies and Results Analysis

In this chapter, different case studies of dynamic frequency control are investigated. The base case study is where only hydro units contribute to the primary frequency control and WTs do not provide FFR. In the second case study, FFR support from WTs is involved as well. Lastly, a coordinated frequency control strategy between WTs and hydro units is developed and evaluated.

6.1 System layout and parameters

One of the 2040 scenarios developed in Chapter 5 is utilized for the purpose of simulation. The NGDP-RS-IWP 2040 looks like an interesting scenario since it has the lowest amount of kinetic energy among the others, with a wind penetration level of 77%. However, according to the FCR-N and FCR-D requirements stated in Sections 2.4.1 and 2.4.2, respectively, there must be at least 600 MW FCR-N and 1200 MW FCR-D in the NSA. In this project we assume a 1450 MW FCR-D capacity to compensate for any uncertainties in the load-frequency damping constant. Moreover, the FCR is provided completely from hydro units. In the considered scenario, the actual hydro generation is 6.6 GWh/h. This corresponds to a maximum capacity of $\frac{6.6\text{GWh/h}}{0.8} = 8.25$ GW assuming 80% loading of the hydro units. This means that (20%)(8.25) = 1.65 GW remains to provide reserve if needed. These are less than the minimum required FCR capacity 1450 + 600 = 2050 MW. This may imply that the average loading of the hydro units will be lowered in such cases where the online capacity of hydro units is low in order to be able to fulfill the FCR requirement. In the NGDP-RS-EWP 2040 scenario, the hydro generation is 11.7 GWh/h, corresponding to $\frac{11.7\text{GWh/h}}{0.8} = 14.6$ GW maximum capacity. 20% out of 14.6 GW gives the hydro spare capacity of 2.9 GW > 2.05 GW, which is sufficient to provide the total FCR. The layout of the system is presented in Figure 6.1. The energy productions at the hour of analysis is constant from the hydro, nuclear, fossil fuel, wind and biomass and are balanced with the load and the net export. Numerical data of the system parameters are listed in Table 6.1. The whole WT capacity in the NSA is assumed to be lumped in one single unit. Starting from this point, the pu power of the lumped WT is given as $\frac{22.1\text{GWh/h}}{54.3\text{GW}}$ = 0.407 pu, where 54.3 GW is the total installed capacity of WTs in the NSA by 2040, according to the NGDP, and 22.1 GWh/h is the actual generation in the given scenario. According to Figure 4.2, the wind speed that yields 0.407 pu is 8.15 m/s, which is the wind speed used as an input to the WT model. However, the 0.407 pu is given with respect to the WT base and need to be converted to the system's base. Therefore, the output of the unit is multiplied by $\frac{S_{\text{bw}}}{S_{\text{b}}}$, where S_{bw} is the online capacity of wind units (54.3 GW) and Sb is the online capacity of all generators in the NSA.

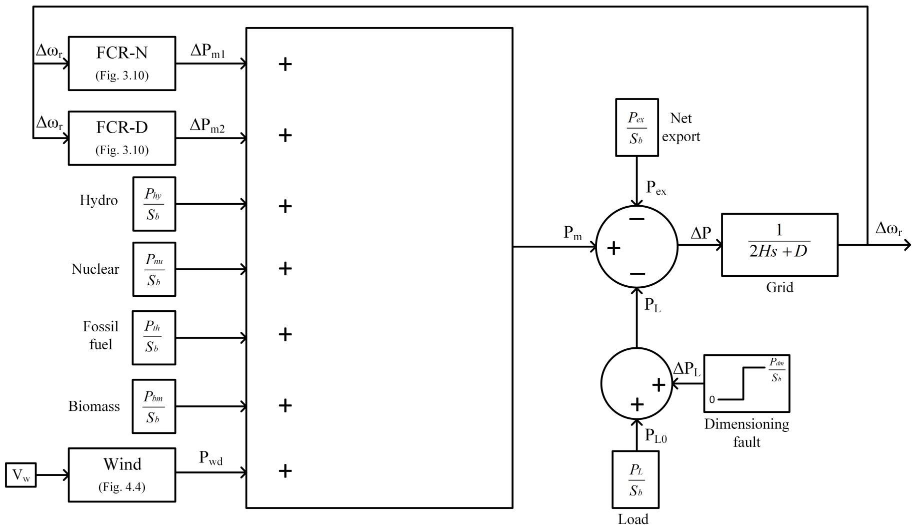

Figure 6.1: System layout with only hydro units contributing to primary frequency control via FCR-N and FCR-D services.

Table 6.1: System parameters

P_{hy}	11.7 GW	H_{pre}	1.76 s	$FCR\text{-}N$	600 MW
P_{nu}	2.1 GW	H_{post}	1.58 s	$FCR\text{-}D$	1450 MW
P_{th}	344 MW	S_b	41.6 MVA	$S_{FCR\text{-}N}$	12000 MW
P_{wd}	22.1 GW	D	0.48 pu	$S_{FCR\text{-}D}$	9667 MW
P_{bm}	470 MW	P_L	34.7 GW	S_{bw}	54.3 GW
V_w	8.15 m/s	P_{ex}	2 GW	P_{dm}	1300 MW

The most important part of this system are the FCR-N and FCR-D models since they are the only source of reserve. These models are given in Figure 3.10. For the governor settings, $EP1$ (see Table 3.2) is seen to be a commonly used setting for FCR-N. The FCR-D settings are usually expected to be faster but this differs from a producer to the other. For instance, producers in Norway use the same governor settings for both FCR-N and FCR-D. Later in this chapter, the usage of different governor settings for FCR-D is investigated. After choosing the governor settings, the online FCR-N and FCR-D capacities can be determined according to (3.12). With 4% droop setting (EP1 setting), the online FCR-N capacity is determined according to

$$S_{\mathrm{FCR-N}} = (0.04)(600\mathrm{MW})(\frac{50\mathrm{Hz}}{0.1\mathrm{Hz}}) = 12000\mathrm{MW}$$

The amount of FCR-N reserve in hundred percent can be calculated as $(\frac{600\mathrm{MW}}{12000\mathrm{MW}})(100\%) = 5\%$. The hydro units are assumed to operate at 80% of their maximum capacity, as given in the hydro model in Section 3.4.2. Therefore, only 15% out of the total capacity is left for the FCR-D. The online FCR-D capacity is calculated assuming EP1 settings as

$$S_{\mathrm{FCR-D}} = (0.04)(1450\mathrm{MW})(\frac{50\mathrm{Hz}}{0.4\mathrm{Hz}}) = 7250\mathrm{MW}$$

However, this value should be checked against the available reserve if it complies or not. The FCR-D in hundred percent is given as $(\frac{1450\text{MW}}{7250\text{MW}})(100\%) = 20\% > 15\%$
This value is greater than the available reserve. One way to solve this problem is by spreading the reserve over a larger amount of hydro capacity. The FCR-D online capacity should be according to

$$S_{\text{FCR-D}} \geq \frac{(1450\text{MW})}{0.15} = 9667MW$$

This can be done by increasing the droop constant to be at least as

$$R_{\text{FCR-D}} \geq \frac{9667\text{MW}}{(\frac{50\text{Hz}}{0.4\text{Hz}})(1450\text{MW})}(100\%) = 5.3\%$$

In this case the regulation strength is unchanged and is given by $\frac{1450\text{MW}}{0.4\text{Hz}} = 3625\text{MW/Hz}$. Another way to overcome this problem is by keeping the droop as 4% and changing the regulation strength instead. In this case the regulation strength should be at least as

$$RS_{\text{FCR-D}} \geq \frac{9667\text{MW}}{(50\text{Hz})(4\%)} = 4834\text{MW/Hz}$$

The main difference between the two methods is that the steady state frequency deviation is different according to (3.5). In addition to that, the dynamic performance is expected to differ slightly. The difference between both methods is discussed in more detail in Section 6.2. Notice that in this project the FCR-D^{max} is assumed 1450 MW rather than the minimum required value (1200 MW). This is because more loads are expected to become converter connected by 2040, hence, less amount of damping power will be available. Nevertheless, the amount of damping constant in 2040 is difficult to predict, thus, it is assumed equal to the current value (400 MW/ Hz). The total hydro capacity needed for FCR-N and FCR-D provision is 12000 MW assuming that 9667 MW of the hydro capacity is providing joint service of both FCR-N and FCR-D. Figure 6.2 illustrates how the FCR-N and FCR-D reserves are distributed among the hydro capacity in the NSA.

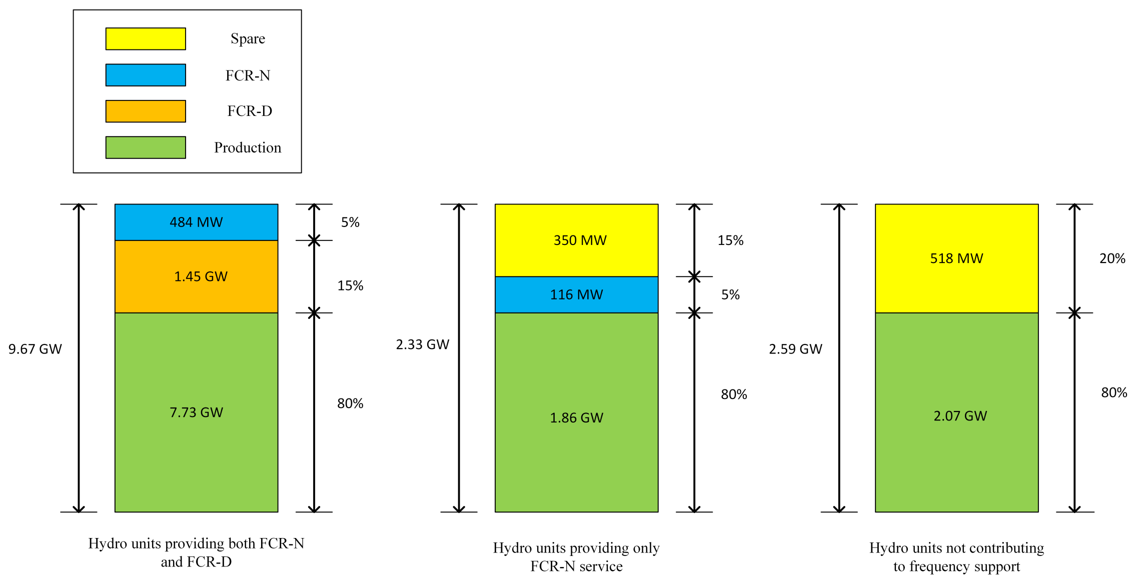

Figure 6.2: FCR-N and FCR-D capacity distribution among hydro units in the NSA.

The dimensioning fault in the NSA by 2040 is expected to be Olkiluoto 3 nuclear unit in Finland with a net capacity of 1600 MW, but it has an attached 300 MW load reducing its tripping power to 1300 MW [16]. The disconnection of such a big unit means that the inertia of the system will decrease. Thus, a step change in the inertia constant must be applied simultaneously with the fault instant. The inertia constant is found to be decreased from 1.76 s to 1.58 s as a result of the tripping of Olkiluoto 3 unit.

6.2 Hydro-based primary frequency control

The system in Figure 6.1 is simulated in Matlab/ Simulink with a dimensioning fault occurring at t=1 s. Figure 6.3 shows the frequency response due to three different governor settings of the FCR-D unit. Details of the used settings and the corresponding parameters of the FCR-D unit are listed in Table 6.2. The fast governor settings are used in [17] for the sake of testing a Swedish kaplan unit. The online FCR-D capacity is calculated in the same way as in Section 6.1, and it yields the same value for all the settings. The main difference between the three settings is in the PI controller and the regulation strength values. It is noticed that the maximum ramp rate limit is reached in all the three settings, therefore, no further improvement in the frequency nadir. This shows how that changing the PI-controller parameters cannot offer vary much in terms of increasing the ramp rate since the kaplan unit has a limited ramp rate. However, the EP1 settings cause less wear and tear than the other settings because it has less cumulative movement distance of the guide vane. Nevertheless, the fast setting with Kp=5 leads to a more damped frequency response, while the EP3 results in an overshoot in frequency above 50 Hz and the EP1 has a frequency overshoot slightly touching 50 Hz. According to [9], the frequency at which automatic load shedding starts in the NSA is 48.8 Hz. This means that the frequency Nadir following a dimensioning fault should be greater than this value by at least some margin. However, the simulation has shown that the frequency Nadir reached 48.56 Hz. It is concluded that using the current hydro-based primary frequency control with slow ramp rate, the system might encounter blackouts following a major disturbance in 2040 due to shortage in system inertia. The EP1 setting for both of FCR-D and FCR-N is used for the rest of the simulations.

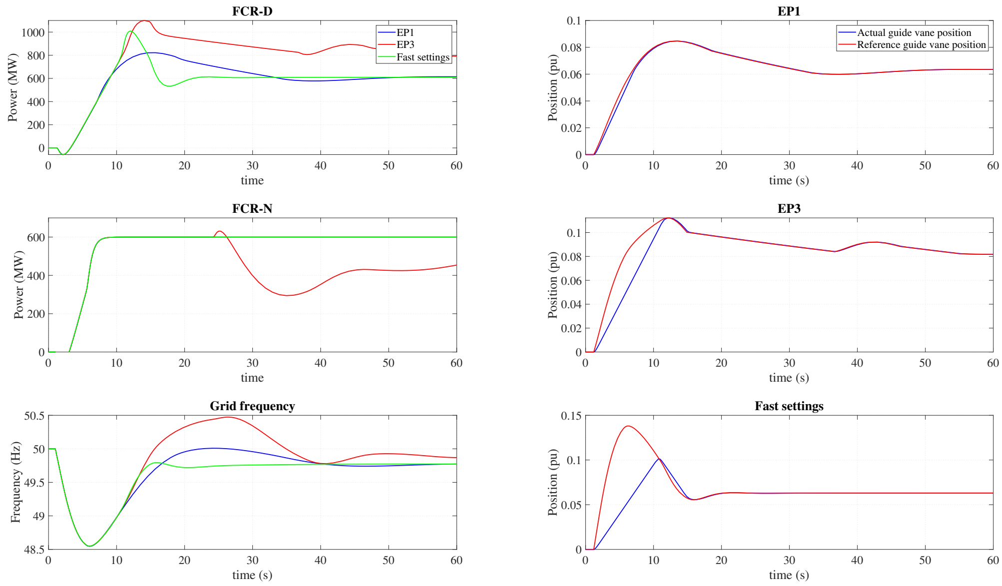

Figure 6.3: Grid frequency and activated reserve after the disconnection of Olkiluoto 3 unit at t=1 s with only hydro units providing frequency support and with respect to three different governor settings of the FCR-D.

Table 6.2: FCR-D parameters

	K_p	K_I	E_p	$FCR\text{-}D^{max}$	$S_{FCR\text{-}D}$	RS
EP1	1	0.42	4%	1450 MW	9667 MW	4834 MW/Hz
EP3	2	0.83	1%	1450 MW	9667 MW	19334 MW/Hz
Fast settings	5	0.6	4%	1450 MW	9667 MW	4834 MW/Hz

One of the parametes that has a great impact on the FCR-D response is the droop settings. Figure 6.4 shows the FCR-D response corresponding to different droop settings. Having a larger droop means that the FCR-D is spread over a greater capacity of hydro units as given by (3.12). This means that not all the 15% dedicated for FCR-D might be really needed in order to provide 1450 MW. It can be seen from the frequency response that the 8% droop has a Superior ramp rate to the others, then comes the 6% droop. This occurs because having more units each pushing less power is faster than having less units each one pushing more power. The FCR-D capacity should not be less than 9667 MW, otherwise, more than 15% reserve will be needed. It is seen that the droop settings of 1%, 4% and 5% has reached this limit, that is why they have quite similar ramp rate. However, the regulation strength of these units is different. A higher regulation strength means having less frequency deviation in steady state as indicated by (3.5). Hence, the setting with 1% droop has less frequency deviation in steady state than others.

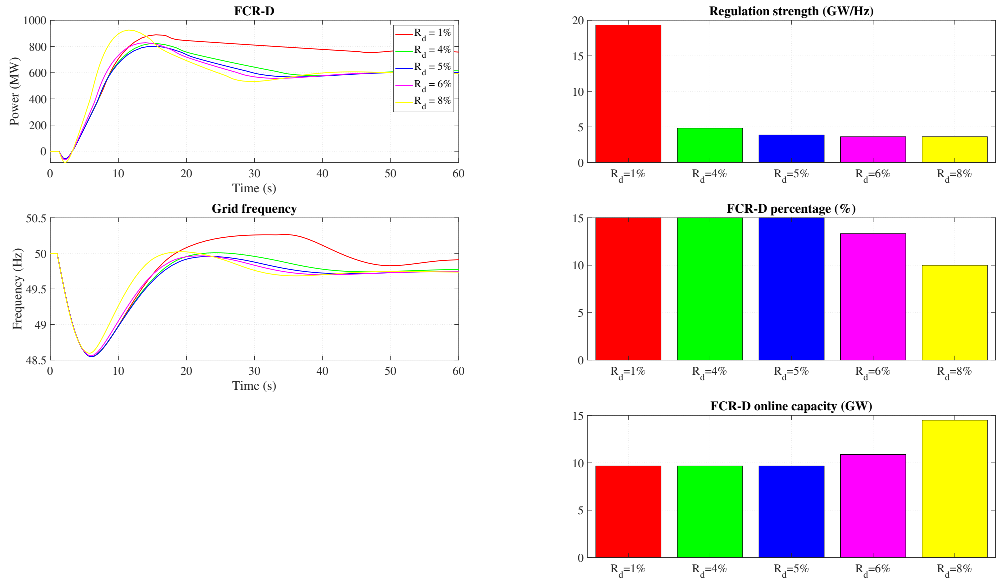

Figure 6.4: Comparison of the frequency response corresponding to different droop settings of the FCR-D.

6.3 WTs participating in fast frequency support

Results in the previous section showed that the frequency nadir following a major disturbance can reach transiently below 49.8 Hz which will trigger load shedding in the NSA as a consequence. Therefore, there is a need for a fast activated reserve to limit this rapid frequency fall. In this section, the system frequency is analysed with respect to two different FFR characteristics, an FFR that is proportional to the RoCoF (synthetic inertia) and an FFR that follows the grid code described in Section 2.5 (predetermined response). Also, the SFD resulting from the recovery of WTs is evaluated with respect to different settings of the inertia provision method.

6.3.1 RoCoF-based inertia provision

A detailed model of the frequency support based on RoCoF is given in Section 4.2.6.

6.3.1.1 Inertia capacity

The inertia capacity is a term used to express the percentage of WTs providing inertial support out of the total WT capacity. Inertia capacity of WTs can play a big role in the frequency response of the Nordic power system. Therefore, the system is analysed with respect to 10%, 25%, 50% and 100% inertia capacities, as shown in figure 6.5. The speed controller is disabled during the inertia provision in this chapter unless said so. The kinetic energy released by the WT shown in the results is defined as

$$\mathrm{KE_{inertia}(t)} = \int_0^t \mathrm{FFR(t)dt}$$

More inertia capacity means better ability at limiting the frequency nadir but this will be accompanied with some oscillations. However, this comes with the cost of extra energy released from the rotor, which might cause a SFD when later recovered. For example, the 100% inertia capacity has at least 13.94 GWs kinetic energy that needs to be recovered by the turbine's rotor. For instance, if this energy is recovered within 10 seconds, this means that 1.394 GW average power is consumed from the grid, which is as worse as the initial fault. It is noticed that the rotor speed is decreasing even after the support has ended. This occurred because the mechanical power is slightly less than the one prior to the fault since the turbine has deviated from its MPP. Further reduction of the rotor's speed will cause the efficiency to reduce even more, and thus the mechanical power will continue decreasing, making it like a positive feedback loop, leading to instability if the speed controller is not activated at the right time. For the rest of the simulations, the 25% inertia capacity is chosen because it make sense that not all the producers would have their WTs contributing to frequency support.

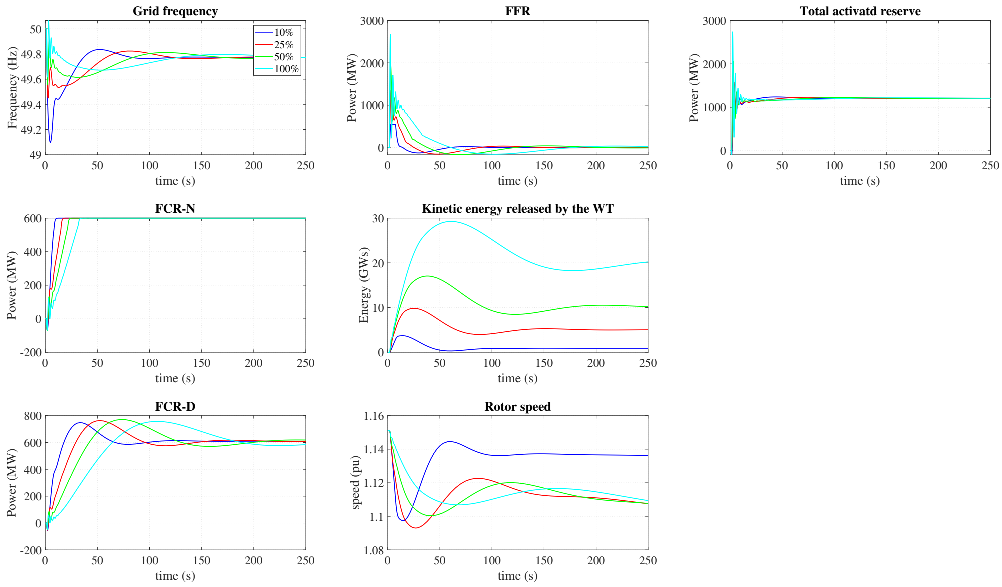

Figure 6.5: Frequency response of the system with respect to different inertia capacities of WTs.

6.3.1.2 Synthetic inertia constant

The inertia provision of a WT is not natural like a conventional generator and thus the synthetic inertia constant is predetermined in the settings. The system is analysed with respect to 2.5 s, 5 s and 7.5 s synthetic inertia constant values. Figure 6.6 shows the frequency response and the activated reserves. The graphs have the same trend as the ones in Figure 6.5, where the idea in both of them is the same, i.e., extra inertia capacity or synthetic inertia constant means more FFR power provided to the system. Anyhow, there is a fundamental difference between the the two cases, while more inertia capacity provides extra energy by increasing the capacity of turbines involved in the support, the excessive energy is provided by the single turbine itself when increasing the synthetic inertia constant. This requires that the rotor's speed deviate even more from its optimal as shown in the figure. Furthermore, since the maximum power of inertia is limited to 0.1

pu, thus, increasing the synthetic inertia constant will not always yield a better frequency response. For example, the FFR is saturated for H_{syn} = 7.5 s. That being the case, having an inertia constant as high as 7.5 s will improve the IFD better, but the kinetic energy that needs to be recovered in this case is higher, which might causes a second dip worse than the first one. But, if the coordination between hydro and wind is done in a good manner then maybe having a high inertia constant value would not be problematic as before. The rest of the simulations are done with the synthetic inertia constant fixed to 7.5 s.

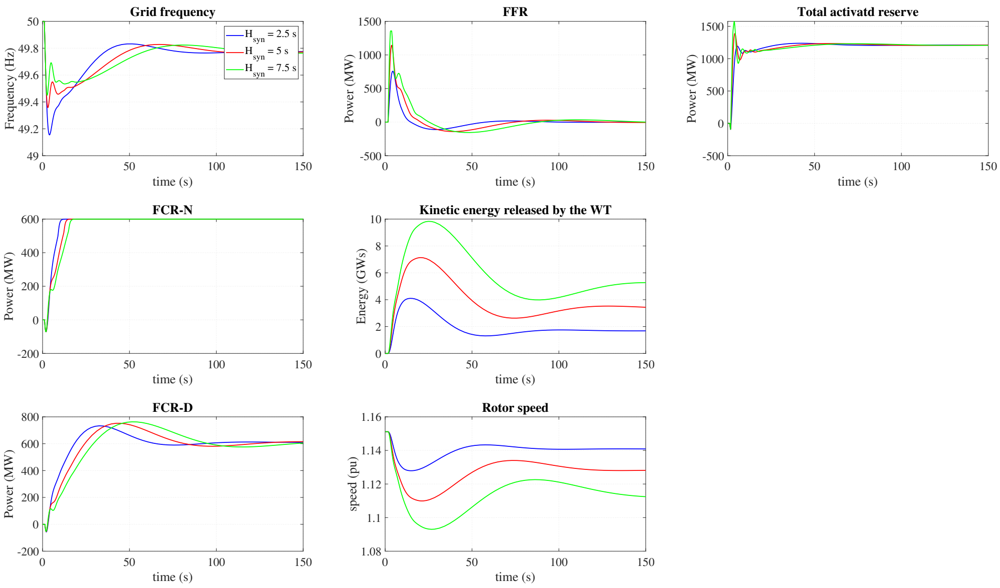

Figure 6.6: Frequency response and activated reserves of the NSA corresponding to a dimesnioning fault at t=1 s and with respect to different synthetic inertia constants.

6.3.1.3 MPPT restoration

In the previous simulations, the speed controller was disabled from the instant of the fault occurrence till the end of the simulation. In the GE report [5], it is recommended that the speed controller should be kept enabled during the support but with reducing the PI controller parameters as discussed in Section 4.2.6. Figure 6.7 shows the system response with the speed controller disabled or enabled during the support duration. It is obvious that enabling the speed controller causes the frequency to be oscillatory. This occurred because of the opposite functionality of the inertia emulation block that is trying to reduce the rotor speed to provide the required support, and the speed controller which is responsible of bringing the speed back to the optimal. Moreover, this contradiction in the functionality of the two blocks causes the turbine to start to recover in an early stage, giving rise to a SFD. Therefore, having the speed controller enabled during the support, even with lower parameters, is not very acceptable. Rather than that, the speed controller is enabled after the support, as will be demonstrated in the next results. In case the rotor speed dropped so much during the support, there is a speed sensor that enables the speed controller as soon as the speed reaches 0.42 pu.

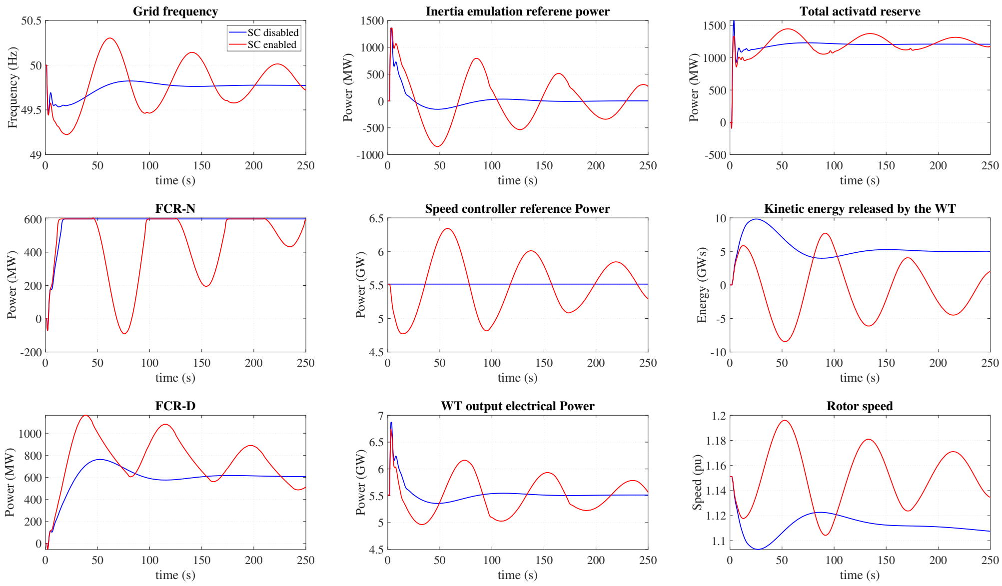

Figure 6.7: Frequency response and activated reserves of the NSA corresponding to a dimesnioning fault at t=1 s with the speed controller enabled or disabled during the support duration.

The speed controller can be frozen during the support and enabled directly after the support ends, as shown in Figure 6.8. In this case, the inertia emulation block is disabled as soon as the deactivation is completed, so there is no common operating time between the speed controller and the inertia emulation blocks. The difference between having a slow and a fast recovery is in the PI-controller parameters of the speed controller. For a fast recovery, the normal MPPT parameters are used (K_p=3 and K_i=0.6), and for the slow operation these parameters are reduced (K_p=0.6 and K_i=0.05). The sudden step change at the activation instant is caused by the proportional controller due to the difference between the rotor speed and the reference speed during the support. Hydro units cannot ramp up their power stepwise, therefore, having a sudden decrease in the FFR will absolutely cause a SFD. But the depth of the dip depends on the time function of the recovery power. The case with the fast recovery have a maximum instantaneous power during the recovery higher than that during the support and it causes the total activated reserve to go transiently into minus. Although the slow recovery has relatively less bump in the frequency, but it has a SFD causing a new frequency nadir. Therefore, both methods are not very acceptable from the TSOs point of view, but the slow recovery can be mitigated by adopting the coordination methods that will be discussed in Section 6.4. It is concluded that although in both cases the energy consumed from the rotor during the support is the same, but how this energy is distributed during the recovery (the power) makes a big difference to the grid frequency.

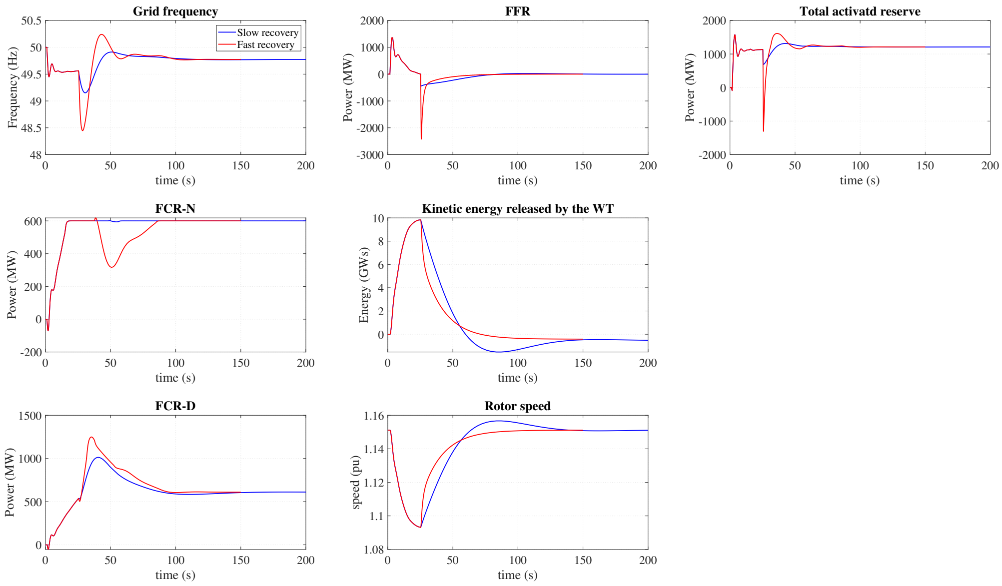

Figure 6.8: Frequency response and activated reserves of the NSA corresponding to a dimesnioning fault at t=1 s, with fast recovery where the normal PI-parameters of the speed controller are used and a slow recovery where the reduced PI-controller parameters are adopted.

One way to mitigate the second dip caused my immediate switching to the speed controller is to delay the recovery power and limit its value. Figure 6.9 shows the frequency response of the case with direct recovery and the new adopted method. According to the FFR technical requirements discussed in Section 2.5, there must be at least a 10 s buffer time before the WT can recover. This shall give some time for hydro units to increase their production. It can be seen that when adopting the buffer time and limitation, the second dip occurs at relatively higher initial frequency and has less amount of frequency deviation. However, the accumulative kinetic energy consumed by the rotor is quite higher because of delayed restoration of the MPP, which causes degradation in the efficiency of the turbine. This can become more precious at low wind speeds when the kinetic energy is less affordable. Later on, the speed controller is enabled when the rotor speed crosses the reference speed, which allows minimum disruption in the power, as clear from the smooth recovery of the FFR towards the MPP starting at around t = 100 s.

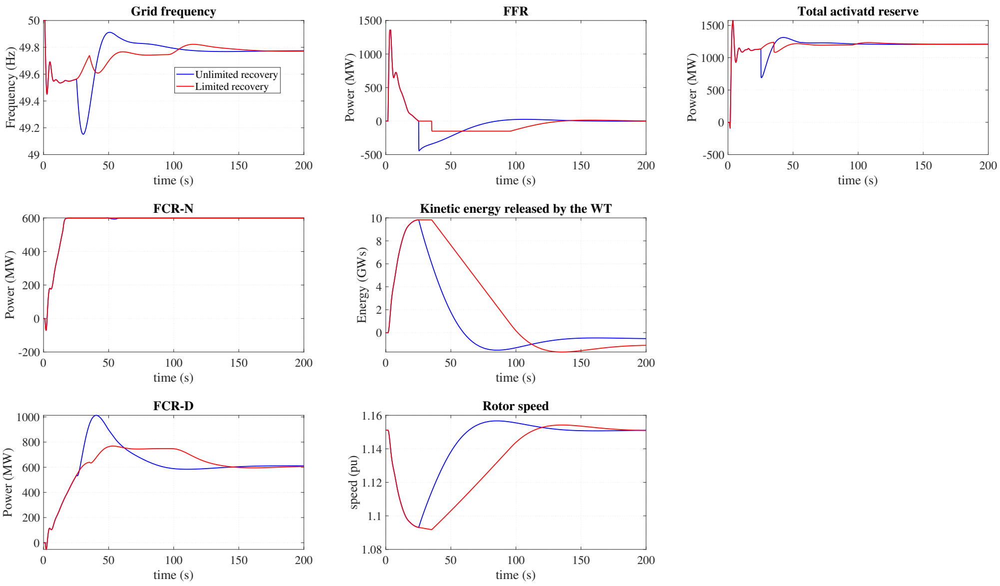

Figure 6.9: Frequency response and activated reserves of the NSA corresponding to a dimesnioning fault at t=1 s utilizing a 10 s buffer time before recovery or neglecting the buffer period.

6.3.2 Predetermined support shape

In this section, an FFR is applied that follows the grid code, and the SFD problem is measured with respect to different sensitivity studies. Refer to Section 2.5 for the FFR requirements.

6.3.2.1 Long and short support duration

Figure 6.10 shows an FFR support that complies to the long support duration requirements. An FFR capacity of 800 MW is applied for 30 s. It is shown in the results that the frequency overshoots when keeping such an amount of FFR capacity for that long. The requirements does not link the duration of the support with the frequency, therefore, a producer who is committed to a long support duration should provide at least 30 s of the prequalified capacity even though if the frequency starts to recover before that. Another observation is that, the FCR-N and FCR-D have only activated 400 MW and 250 MW of their reserves, respectively. This occurred because the frequency have been restored quickly by the FFR. Following the deactivation a SFD occurs almost approaching 49 Hz. This can be attributed to the fact that the deactivation of FFR is applied instantly while not enough FCR-N and FCR-D reserves are activated. Yet there is no clue about the FFR capacity in the grid code, but according to these results it is shown that applying a long fixed support capacity as large as 800 MW can cause frequency instability. After the deactivation, a 10 s buffer period is devoted before the recovery starts. This buffer time allows the FCR to increase its production, which makes the recovery inferior in causing a frequency dip especially that it is limited to 25% of the FFR capacity (200 MW in this case). However, during the support duration, the mechanical power of the wind turbine has reduced because of the reduction of the efficiency. It is observed that the mechanical power is slightly higher than the electrical power during the recover, which makes the rotor speed approaches the MPP very slowly. If the support lasted more than 30 s the mechanical power may drop even more such that 200 MW of recovery may not be enough to restore the rotor speed. This poses another question on the FFR requirements.

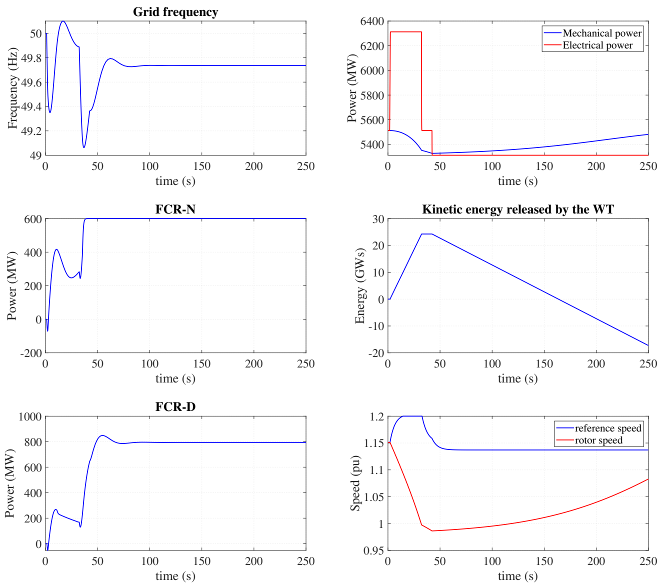

Figure 6.10: The frequency response when applying a long support duration FFR of 800 MW capacity.

Figure 6.11 shows a comparison between having a long and a short support duration from WTs. The comparison is made such that each support provides the same amount of energy, with the short support capacity equal to 800 MW applied for 5 s and the long support capacity is 133 MW for 30 s. By spreading the FFR energy over a longer time period, the ability to arrest the initial frequency drop becomes less with the frequency falling below 49 Hz. On the other hand, by pushing all the FFR energy in the first 5 seconds, the IFD is improved (49.35 Hz), but the amount of activated FCR-N and FCR-D is reduced. However, in the case with short support duration a SFD occurs following the deactivation but it is not so significant as compared to the SFD in Figure 6.10. The reason for this is that here the deactivation rate is 20% of the FFR capacity per second, while in the previous result the deactivation takes place instantly. These deactivation rates were applied according to the requirements, which state that the deactivation rate should not be more than 20% of the FFR capacity per second if short support is utilized, while it can be stepwise if the entity is committed to long support duration. By slowing down the deactivation, hydro units can increase their FCR, thus, the SFD becomes less severe. Nevertheless, the long support duration in Figure 6.11 does not cause a SFD although it has a stepwise deactivation shape. This occurred because the amount of FFR power is 133 MW which is much less than 800 MW, therefore, there is no need for slowing down the deactivation in this case.

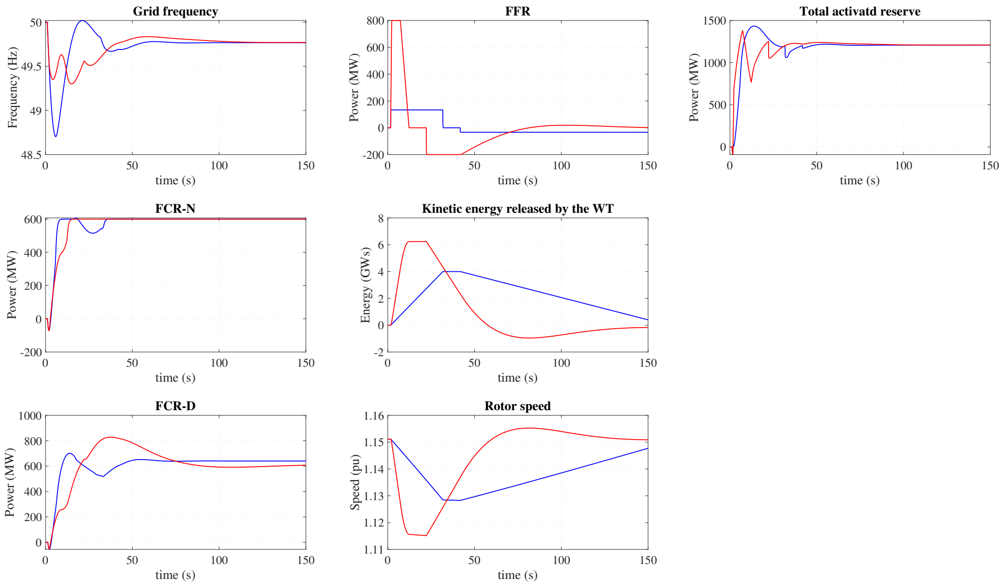

Figure 6.11: A comparison between the frequency response of a long and short support duration with equivalent support energy.

6.3.2.2 FFR capacity

In this section, a sensitivity analysis with respect to the FFR capacity is presented. Figure 6.12 shows the frequency response with respect to 600 MW, 800 MW and 1000 MW FFR capacities applied for 5 s (short support duration). The capacity of FFR providing WTs is 25% of the total wind capacity, which corresponds to (25%)(54.3 GW) = 13.6 GW. Therefore, the FFR capacities in this example correspond to 4.4%, 5.9% and 7.4% of the inertia capacity. The results show that even though the IFD is improved with a higher FFR capacity, the SFD becomes worse. In the case with 600 MW the SFD is less than the initial one, in the 800 MW case it becomes slightly worse than the initial dip and in the 1000 MW case it starts becoming much worse than the initial dip. The reason for this is that as the amount of support power increases, the amount of energy needed for the WTs to recover will become more as well. Moreover, the rate of deactivation here is applied based on the maximum limit in the requirements (20% per second of the FFR capacity). Therefore, the deactivation rate increases as the support power increases, which makes the second dip even worse.

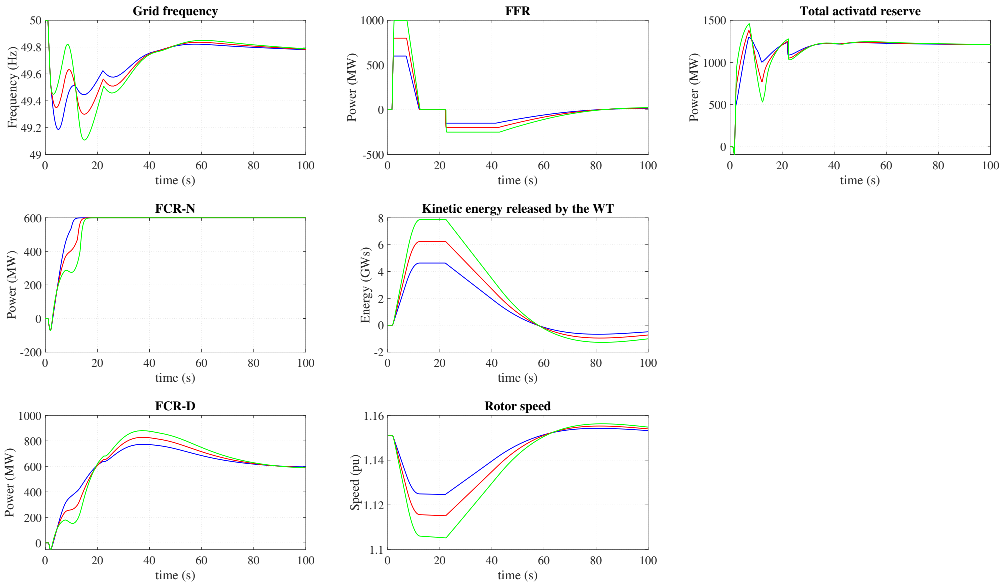

Figure 6.12: Frequency response corresponding to different FFR capacities of short support duration.

6.3.2.3 Deactivation rate

In this section, the frequency response is studied with respect to different deactivation rates. The maximum deactivation rate in the FFR requirements is 20% of the FFR capacity per second. Figure 6.13 shows the frequency response with respect to 10%, 20% and 100% deactivation rates with an 800 MW FFR capacity. It is clear from the figure that the SFD becomes less significant as the deactivation rate is reduced. The case with 100% deactivation rate exceeds the limitation imposed in the requirements and it shows a tendency of the frequency to fall down rapidly compared to other cases. By applying the maximum deactivation rate in the requirements (20%), the SFD is almost as significant as the initial dip. When increasing the duration of deactivation, the FCR will have more time to rise, thus, the SFD is mitigated. Therefore, according to the results in Figures 6.12 and 6.13, both the FFR capacity and the deactivation rate can determine the significance of the SFD.

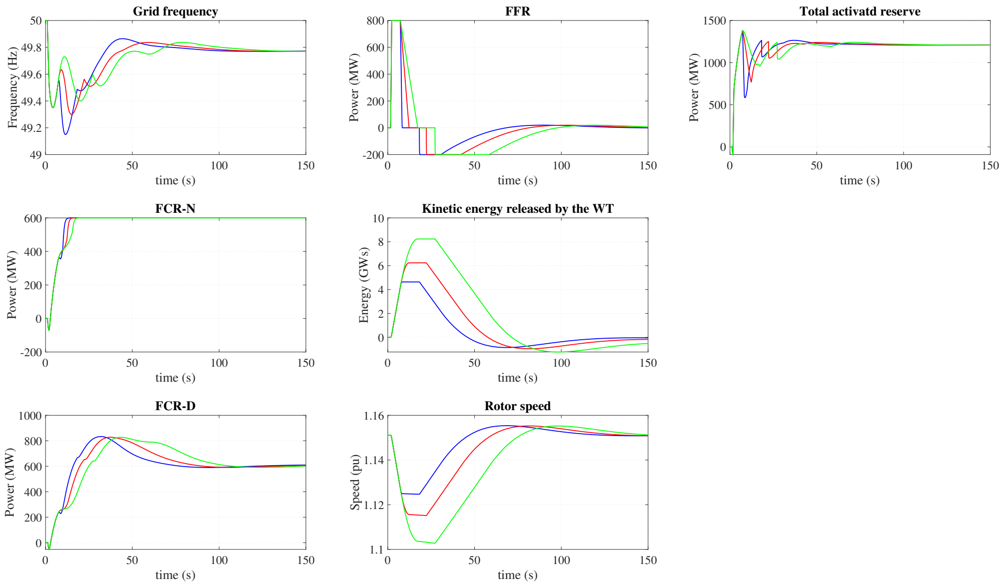

Figure 6.13: Frequency response corresponding to different deactivation rates of an 800 MW FFR with short support duration.

6.4 Coordinated frequency support provision

As have been seen in the previous section, the activated reserves are capable of restraining the IFD caused by the disturbance. However, during the WT's recovery period of the synthetic inertia support or the deactivation period of the predetermined support, a SFD might occur, which sometimes become even more severe than the initial one. In this section, the possibility of mitigating the SFD or even eliminating it, is investigated by controlling hydro units to ramp up more power in coordination with WTs. As discussed in Section 3.2, the mechanical power reference of the hydro units can be modified by adding an additional power signal to produce additional power from the hydro units to mitigate the SFD. But the question is, when to send this signal? and when to remove it? and what should this signal be based on? The coordination block diagram that is adopted in this project is shown in Figure 6.14. The LSP signal is determined by the frequency deviation, such that it becomes positive if the frequency deviation is more than 0.1 Hz, otherwise, the deadband block cuts the signal to zero. The importance of the deadband is to prevent overshoot in frequency that might arise due to high LSP reference signal. An important aspect in the coordination process is the time instants at which the coordination starts and ends. These times instants are determined by a communication signal which is a zero/one signal being sent by the WT corresponding to a specific stage in the FFR provision. The FFR characteristics can play a big role in allocating the communication period. Another improtant factor in the coordination process is the LSP gain, which determines how much and how fast the hydro unit can respond to a LSP reference signal. The LSP gain determines the volume of the coordination and choosing it depends on the FFR characteristics such as the FFR capacity, deactivation rate, the recovery power and its rate.

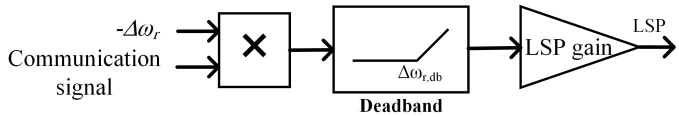

Figure 6.14: Coordination block diagram going to the LSP of the hydro model in Figure 3.10.

An interesting scenario for coordination is to have the recovery starting right away after the deactivation ends and to be a stepwise recovery, as shown by the case without coordination in Figure 6.15. In this case, the SFD occurs due to the recovery, when the turbines tries to re-accelerate. The SFD in this scenario is greater than the initial dip. One solution for the SFD was presented in Figure 6.9, which is to use a buffer time and limit the recovery power. However, this solution makes the recovery of the turbine much slower, which is something unfavourable by the WT producer. Another way to solve the SFD is to employ the coordination method. Since hydro units cannot increase their power instantly, and because the recovery of the the WT is stepwise, the coordination should be initiated prior to the recovery. Here, the start of deactivation is used as a reference for the initiation of the LSP signal. By doing so, the deactivation will last shorter because it is dependent on the RoCoF. Thus, the recovery will start earlier than before. Ideally, the recovery will start when the RoCoF is equal to zero, which means that the power mismatch at this moment is also equal to zero according to the swing equation (3.1). Therefore, any attempt to activate more power prior to the recovery will only accelerate the deactivation and will not serve in increasing the power mismatch. But bear in mind that the synthetic inertia support is based on a high pass filter with a time constant of 5.5 s. Hence, the recovery instant occurs some time after the frequency nadir takes place. As a consequence, the power mismatch in the swing equation becomes positive prior to the recovery. The LSP signal is then removed at the instant of recovery. The motivation for this is that the recovery power goes down just instantly and then it starts to increase. Moreover, keeping the LSP signal for a longer time may cause an overshoot in frequency so it has to be removed at the right time. In the figure, it is shown that hydro was capable of mitigating the second dip to a large extent in a way it became less than the initial dip. Also, it is shown that the frequency approaches the steady state smoothly without any overshoot. Another important notice is that the FCR-D rate limiter was saturated during the coordination. The maximum ramp rate limit of FCR-D is 0.011 $\frac{\text{pu}}{\text{s}}$ $\times$9667 MW = 106 MW/s. Thus, knowing that the ramp rate is limited, the instant at which coordination starts should be chosen wisely in order for the coordination to be effective. Another advantage of this method is that the recovery can start earlier, resulting in less amount of kinetic energy released from the rotor. This can become more beneficial in cases where the wind speed is low. This method of coordination has proven its ability to mitigate the SFD effectively, causes less deviation in the rotor speed and recovers earlier. Therefore, improving the frequency quality and at the same time utilizes the WT's rotor kinetic energy more efficiently.

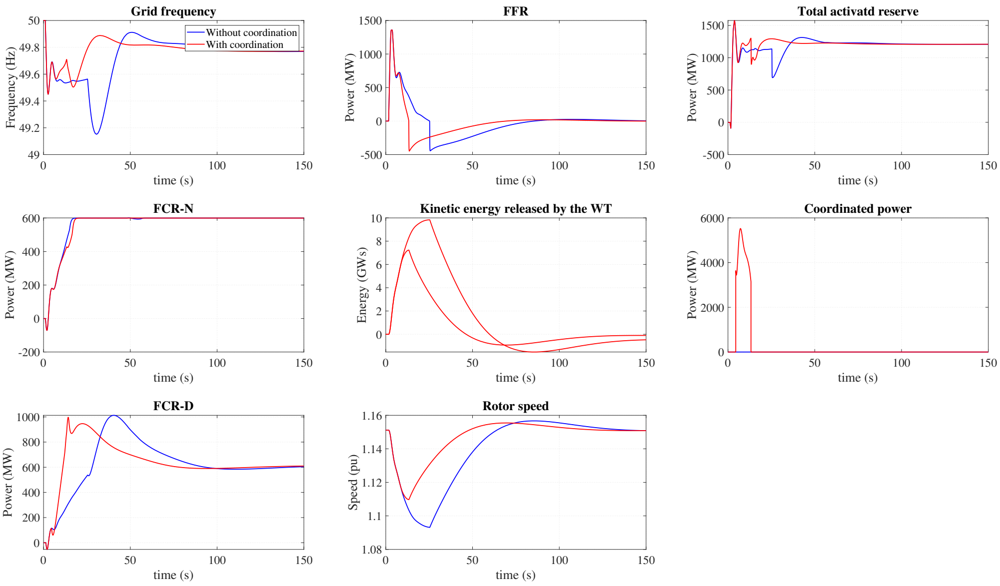

Figure 6.15: A comparison between the frequency response with and without coordination corresponding to direct stepwise recovery of WTs.

Another way to mitigate the SFD is by slowing down the recovery of WTs. This method is demonstrated in Figure 6.16, where the power converter time constant is changed from 0.05 s to 10 s during the recovery. Although the WT recovery is made slower, yet the second dip is still more significant than the initial one. The recovery period has two parts, one when the recovery power is decreasing and the other part when the recovery power starts increasing (approximately when the rotor speed exceeds the reference speed). At the moment the recovery starts, hydro units receive a command from WTs to increase their production. The recovery power is slow in this case and thus, hydro units can increase their power simultaneously while the recovery takes place. It can be observed that the SFD is eliminated totally because the FCR-D is increased at a faster rate than the recovery was decreasing, except for the first few seconds due to the negative phase of hydro units. The LSP is then removed when the rotor speed exceeds the reference speed for the first time. This moment is roughly at which the FFR power starts increasing. Thus, by removing the coordinated power at this time instant, the FCR-D starts reducing at the same moment the WTs start increasing their power. However, FCR-D is reduced faster than the FFR is increasing, causing a frequency dip but is relatively smaller and occurs at a higher frequency compared to the original dip in the case without coordination. As a conclusion, it is difficult to control the instantaneous power of hydro turbines due to the time delay required to increase production after sending the LSP reference signal. This makes simultaneous coordination challenging.

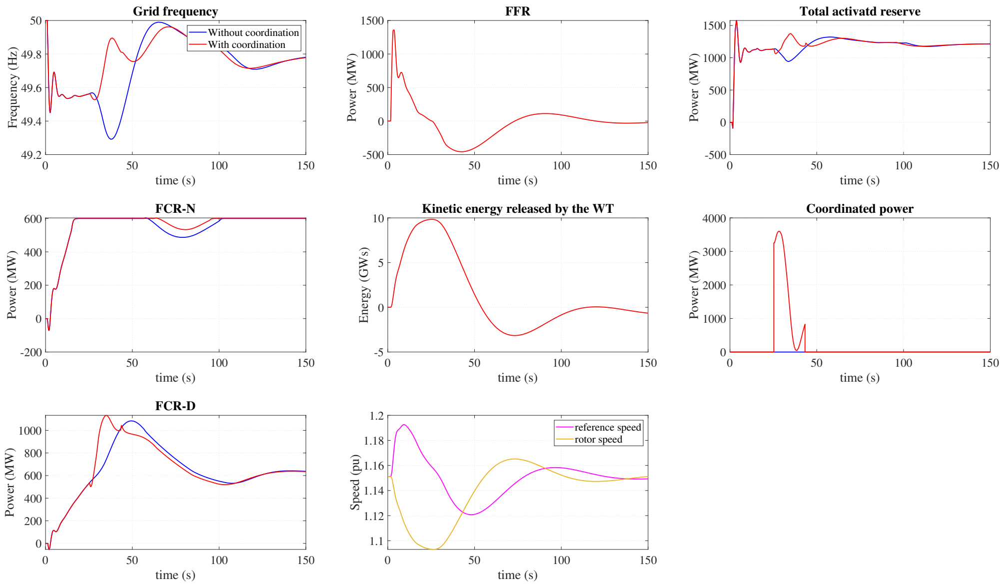

Figure 6.16: A comparison between the frequency response with and without coordination corresponding to slow recovery of WTs.

One of the interesting cases when sensitivity analysis was done in Section 6.3.2 is when the FFR support is 1000 MW with a deactivation rate of 20%. Figure 6.17 shows the frequency response corresponding to the case with and without coordination. The communication signal is sent when the WT starts to deactivate its FFR, which is the main event causing the SFD, and then removed upon the end of the deactivation. By utilizing coordination, the SFD has improved from 49.11 Hz to 49.4 Hz. However, the FFR deactivation rate is 200 MW/s while the maximum FCR-D ramp rate is 106 MW/s, which makes it difficult to eliminate the SFD but rather than that it is mitigated. As discussed in Section 6.2, the ramp rate of the single hydro unit cannot be increased since it is a property of the unit itself, and the overall ramp rate can be improved by increasing the FCR-D capacity such that more units push power with each one having less reserve. But during high wind speeds the online hydro capacity is at its minimum, therefore, this technique becomes less relevant. Another suggestion is to reduce the deactivation rate, which has proven, according to the results in Section 6.3.2.3 to be an effective solution on its own.

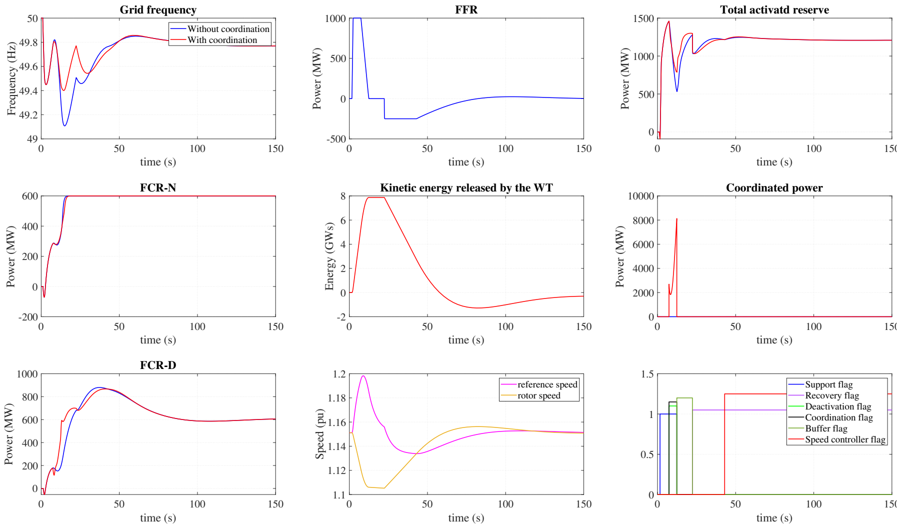

Figure 6.17: A comparison between the frequency response with and without coordination corresponding to an FFR of 1000 MW capacity and a short support duration.

Through out this chapter, different sensitivity analysis has been done, and different strategies to improve the IFD and/or SFD have been evaluated. Table 6.3 lists the impact of different parameters and strategies on the IFD and SFD.

Table 6.3: A summary of the different parameters and strategies analysed in this chapter and their impact on the IFD and the SFD.

Parameter/strategy	Impact on IFD	Impact on SFD
Inertia capacity	Increased inertia capacity will improve the IFD.	The SFD becomes worse as more inertia capacity is incorporated.
Synthetic inertia constant	Increasing the synthetic inertia constant will improve the IFD unless the inertia capacity limit is reached (0.1 pu).	An increase in the synthetic inertia constant results in a larger SFD.
PI-parameters of the speed controller	No impact (considering that the speed controller is frozen during the support).	Using a slower PI-controller parameters during recovery will improve the SFD.
Buffer time and limited recovery	No impact. The buffer time and the recovery take place after the IFD.	Utilizing a buffer time and limiting the recovery power can reduce the SFD effectively.
FFR capacity	Higher FFR capacity can mitigate the IFD.	Increased FFR capacity results in a worse SFD.
Deactivation rate	No impact. Deactivation occurs after the IFD.	Slowing down the deactivation can mitigate the SFD.
Coordinated power control	No impact. It aims to tackle the SFD problem.	It has the ability to mitigate the SFD or even eliminate it.

7

Conclusions and Future Work

In this project, a coordinated control strategy between hydro and wind turbines is developed aiming to provide a fast frequency reserve to reduce the IFD following a disturbance while mitigating the potential second frequency dip that occurs due to the restoration phase of WTs. In order to evaluate the performance of the coordinated control strategy, the system is analyzed in MATLAB/Simulink. The hydro model is represented using a simplified linear Kaplan model, while WTs are characterized with a VSWT GE model with MPPT control during normal operation and an inertia provision control during disturbed operation. The system is modeled by the swing equation with the inertia constant estimated based on a 2040 windy summer scenario of the NSA where the system inertia is relatively low.

It is noted from the simulations that the future Nordic power system has less inertia and the current hydro-based primary frequency control may not be able to meet the minimum frequency nadir requirements of such a system. Providing an FFR from WTs can mitigate the IFD effectively, but a SFD may arise. The SFD is very dependent on the support power and the deactivation rate in case of a grid-code based FFR support or on the recovery power and its ramp rate if RoCoF-based support is utilized. A frequency support based on the grid code can cause two additional dips, one that is associated with the deactivation and the other is related to the recovery. The deactivation strategy is better if it is based on RoCoF to mitigate the second frequency dip. If the deactivation strategy is independent of RoCoF as in the grid code, a second frequency dip may become severe. The SFD can be mitigated by either adopting a buffer time and limiting the recovery power, or coordinating with hydro to provide additional temporary power support. Since the main purpose of coordination is to mitigate the SFD, a coordinated power proportional to the frequency deviation is adopted. This coordination is initiated prior to the event causing the SFD and its volume is dependent on the severity of the event. One of the challenges when it comes to the coordination is the ramp rate of hydro units. The FCR maximum ramp rate is dependent on the FCR online capacity and the hydro unit capability. Therefore, in cases where deactivation rates of WTs is faster, extra ramp rate may be needed while it is unaffordable. Moreover, controlling the instantaneous power of hydro turbines is difficult, due to the time delay until the turbine generates power when given a LSP reference signal. This imposes another challenge on committing the coordinated control method.

Suggested future work includes:

- Impact of electrical distance
  Although the frequency is the same in a synchronized system, but during a disturbance, the frequency might differ transiently between different areas. In order

to evaluate the impact of this phenomena on the coordinated support strategy, the system is represented with the tie line model according to [6]. In this model, each area is represented by its equivalent swing equation and a line impedance reflects the electrical distance between them.

- Evaluate the stability of the controller
  The stability of the coordinated control method should be verified. This can be done by injecting a sinusoidal frequency sweep as a disturbance to the system to check for any unstable behavior and/or analytical analysis based on transfer functions.

- Variable wind speed
  The wind speed in this project is considered fixed during the primary frequency support period (approximately 2 mins). Case studies can be done here, such as if wind speed reduces by 1m/s at the beginning of the support or when recovery starts. In the first case, the rotor speed will drop faster and may lead to stall before support ends. While in the second case, it may be required that the WT absorbs more power from the grid in order to be able to recover, making the SFD even worse.

- Sensitivity analysis of the damping constant
  In the future power system, there will be a shift towards converter interfaced loads. Therefore, the damping power of the system will reduce. Thus, more damping power will also be needed to mitigate power oscillations.

- Frequency deviation-based FFR support
  According to research, the SFD problem is more evident when providing FFR based on the frequency deviation. Using this method, the IFD can be improved much better, but the energy utilized from the rotor will be increased. Thus, it might be useful to apply the coordinated control with such a case.

- Windy and sunny summer day scenario
  In this project, the capacity of PV cells is neglected. However, PV power may constitute a few percents of the total production energy especially during a sunny day. Both WTs and PV cells do not contribute to the system inertia. Thus, a windy and sunny day in summer would have even less inertia and the hydro capacity in this case will also decrease.

- Wind turbine electrical efficiency
  The efficiency of the electrical generator of the wind turbine is neglected in this project. However, adding up the losses means extra reference power is needed in order to deliver the same FFR power. This will result in consuming more energy from the rotor's kinetic energy and the turbine may reach stall condition faster.

- A very windy summer day
  The wind penetration level in this project is 60%. In a case of a very windy summer day, the wind penetration level may reach 80%. This may result in reducing the online hydro capacity. Thus, hydro units may need to reduce their production below

80% in order to be able to provide the required FCR capacity. This scenario will add two extra difficulties, first the inertia is low due to high wind penetration levels and second the FCR ramp rate may become slower because of less online hydro capacity.

- Performing a laboratory test
  Performing a lab test is important in order to verify the simulation results.

Bibliography

[1] N. Modig, R. Eriksson, L. Haarla, et al. “Technical Requirements for Fast Frequency Reserve Provision in the Nordic Synchronous Area,” ENTSO-E, Tech. Rep., 2019. [Online]. Available: https://www.entsoe.eu/publications/system-operations-reports/#nordic

[2] M. Kuivaniemi, N. Modig, R. Eriksson. “FCR D design of requirements,” ENTSO-E, Tech. Rep., 2017. [Online]. Available: https://www.entsoe.eu/publications/system-operations-reports/#nordic

[3] R. Eriksson, N, Modig, A. Westberg. “FCR-N Design of requirements,” ENTSO-E, Tech. Rep., 2017. [Online]. Available: https://www.entsoe.eu/publications/system-operations-reports/#nordic

[4] E. Weihs. “Wind power penetration levels impact on net load variations using an inverse grid model.” M.A. thesis, Chalmers University of Technology, Sweden, 2019. [Online]. Available: https://hdl.handle.net/20.500.12380/300072

[5] K. Clark, N. W. Miller, J. J. Sanchez-Gasca. “Modeling of GE Wind Turbine-Generators for Grid Studies,” GE Energy, Tech. Rep., 2010.

[6] P. Kundur. *Power System Stability and Control.* New York, NY: McGraw-Hill, 1994.

[7] E. Ørum, L. Haarla, M. Kuivaniemi. “Future System Inertia 2,” ENTSO-E, Tech. Rep.. [Online]. Available: https://www.entsoe.eu/publications/system-operations-reports/#nordic

[8] M. Persson. “Frequency Response by Wind Farms in Power Systems with High Wind Power Penetration.” Ph.D. dissertation, Chalmers University of Technology, Sweden, 2017. [Online]. Available: https://research.chalmers.se/publication/250313

[9] “System Operation Agreement appendices,” ENTSO-E, Tech. Rep., 2017. [Online]. Available: https://www.entsoe.eu/publications/system-operations-reports/#nordic

[10] “ENTSO-E transparency platform,” ENTSO-E, 2019. [Online]. Available: https: //-transparency.entsoe.eu

[11] “Nordic Grid Development Plan 2019,” Statnett, Fingrid, energinet, Svenska Kraftnät, Tech. Rep., 2019 [Online]. Available: https://www.svk.se/siteassets/om-oss/rapporter/2019/nordic_grid_development_plan2019.pdf

[12] “LÅNGSIKTIG MARKNADSANALYS 2018,” Svenska Kraftnät, Tech. Rep., 2019 [Online]. Available: https://www.svk.se/siteassets/om-oss/rapporter/2019/langsiktig-marknadsanalys-2018.pdf

[13] “TYNDP 2018 – Scenario Report Annex 1” ENTSO-E, ENTSO-G, Tech. Rep.. [Online]. Available: https://tyndp.entsoe.eu/tyndp2018/scenario-report/

[14] “Nuclear Power in Finland,” World Nuclear Association, 2020. [Online]. Available: https://www.world-nuclear.org/information-library/country-profiles/countries-a-f/finland.aspx

[15] J. Näsström. “State-of-the-art development platform for hydropower turbine governors.” M.A. thesis, umeå university, Sweden, 2017. [Online]. Available: http://www.diva-portal.org/smash/get/diva2:1173833/FULLTEXT01.pdf

[16] “Challenges and Opportunities for the Nordic Power System”, statnett, Fingrid, energinet, Svenska Kraftnät, Tech. Rep..

[17] E. Dahlborg, P. Norrlund, L. Saarinen, U. Lundin. (2019, Oct). “Improving frequency control from kaplan turbines to fulfill grid codes.” *HYDRO 2019*. [Online]. Available: https://www.diva-portal.org/smash/get/diva2:1373955/FULLTEXT01.pdf

[18] W. Yang, P. Norrlund, L. Saarinen, et al. “Renewable Energy.” *Wear and tear on hydro power turbines e Influence from primary frequency control*, vol. 87, pp. 88-95, Oct. 2015.